Institute of Animal Pathology, Department of Infectious Diseases and Pathobiology,
Vetsuisse Faculty University of Bern

Director Head of Institution: Prof. Sven Rottenberg

Scientific supervision was provided by
Prof. Sven Rottenberg and Dr. Simone de Brot

Artificial Intelligence and Immunohistochemical Analysis of the *BRAF V595E* Mutation in Canine Lower Urinary Tract and Prostate Tumors

Inaugural Dissertation

To be awarded the Doctoral Degree of the
Vetsuisse Faculty University of Bern

submitted by

Bettina Leonore Aeschlimann

Veterinarian
born in Fribourg/CH

2024

Approved by the Vetsuisse Faculty as inaugural dissertation on proposal from
Prof. Sven Rottenberg and
Dr. Simone de Brot

Bern, Dean of the Vetsuisse Faculty University of Bern

Table of contents

Vetsuisse Faculty University of Bern, 2024

Leonore Aeschlimann, Institute of Animal Pathology

Email address of the institutional secretariat: christine.herzig@unibe.ch

Artificial Intelligence and Immunohistochemical Analysis of the *BRAF V595E* Mutation in Canine Lower Urinary Tract and Prostate Tumors

Summary

Canine urothelial carcinoma (UC) and prostate carcinoma (PC) frequently exhibit the $BRAF^{V595E}$ mutation, akin to the $BRAF^{V600E}$ mutation common in various human cancers. Since the initial discovery of the *BRAF* mutation in canine cancers in 2015, PCR has been the standard method for its detection in both liquid and tissue biopsies. During the scope of this doctoral thesis, we evaluated two different techniques for detection of $BRAF^{V595E}$ in tumors of the canine lower urinary tract and prostate.

Recent advances in digital pathology and the power of artificial intelligence (AI) have opened up new possibilities for the detection of genetic alterations through AI histology, and offer a wide range of new opportunities in the field of diagnostic and predictive tumour marker detection. The aim of the first study was to test the efficacy of AI histology to predict the presence of $BRAF^{V595E}$ in canine bladder carcinomas and to assess its intratumoral heterogeneity. We used a commercially available AI histology software to predict $BRAF^{V595E}$ in whole slide images (WSI) of bladder UC stained with haematoxylin and eosin (HE), based on a training (n = 81) and a validation set (n = 96). Among 96 WSI, 57 showed identical PCR and AI-based *BRAF* predictions, resulting in a sensitivity of 58% and a specificity of 63%. The sensitivity increased substantially to 89% when excluding small or poor-quality tissue sections. Test reliability depended on tumour differentiation ($p < 0.01$), presence of inflammation ($p < 0.01$), slide quality ($p < 0.02$) and sample size ($p < 0.02$).

This is the first study to utilize AI histology to predict *BRAF* mutational status in canine UC.

Considering the similarity between the canine $BRAF^{V595E}$ and human $BRAF^{V600E}$ mutations, we hypothesized that immunohistochemistry (IHC) using a $BRAF^{V600E}$-specific antibody could effectively identify the canine mutant $BRAF^{V595E}$ protein. For this second study, we tested 122 canine UC (bladder n=108, urethra n=14) and 21 PC using both IHC and digital droplet PCR (ddPCR) and included benign tissue as control as well. The results from ddPCR and IHC were concordant in 99% (135/136) of the tumors. Using IHC, $BRAF^{V595E}$ was detected in 72/122 (59%) UC and 14/21 (65%) PC. Staining of all benign bladder and prostate tissues was negative. If present, mutant BRAF staining was homogenous, with rare intratumor heterogeneity in three (4%) cases of UC. $BRAF^{V595E}$ was more prevalent in tumors with urothelial morphology, and less common in glandular PC or UC with divergent differentiation. This study establishes that $BRAF^{V600}$-specific IHC is a reliable and accurate method for detecting the mutant $BRAF^{V595E}$ protein in canine UC and PC. Moreover, the use of IHC, especially with tissue microarrays, provides a cost-efficient test for large-scale screening of canine cancers for the presence of *BRAF* mutations. This advancement paves the way for further research to define the prognostic and predictive role of this tumor marker in dogs and use IHC to stratify dogs for the treatment with BRAF inhibitors.

Keywords: Urothelial carcinoma, prostate carcinoma, BRAF, artificial intelligence, immunohistochemistry, PCR

animals

MDPI

Article

Artificial intelligence to predict the *BRAF*^{V595E} mutation in canine urinary bladder urothelial carcinomas

Leonore Küchler [1,*], Caroline Posthaus [1], Kathrin Jäger [2,3], Franco Guscetti [4], Louise van der Weyden [5], Wolf von Bomhard [6], Jarno M. Schmidt [7], Dima Farra [8], Heike Aupperle-Lellbach [2,3], Alexandra Kehl [2,3], Sven Rottenberg [1,9,10] and Simone de Brot [1,9,10,*]

1 Institute of Animal Pathology, Vetsuisse Faculty, University of Bern, 3012 Bern, Switzerland; caroline.posthaus@unibe.ch (C.P.); sven.rottenberg@unibe.ch (S.R.)
2 Laboklin GmbH & Co. KG, 97688 Bad Kissingen, Germany; jaeger@laboklin.com (K.J.); aupperle@laboklin.com (H.A.-L.); kehl@laboklin.com (A.K.)
3 Institute of Pathology, Department of Comparative Experimental Pathology, School of Medicine, Technical University of Munich, 81675 Munich, Germany
4 Institute of Veterinary Pathology, Vetsuisse Faculty, University of Zurich, 8057 Zurich, Switzerland; franco.guscetti@vetpath.uzh.ch
5 Wellcome Sanger Institute, Cambridge CB10 1SA, UK; lvdw@sanger.ac.uk
6 Synlab Vet Animal Pathology Munich, 81477 Munich, Germany; wolf.vonbomhard@synlab.com
7 Small Animal Clinic Hofheim, 65719 Hofheim, Germany; jarnoschmidt@googlemail.com
8 Veterinary Public Health Institute, Vetsuisse Faculty, University of Bern, 3012 Bern, Switzerland; dima.farra@unibe.ch
9 COMPATH, Vetsuisse Faculty, University of Bern, 3012 Bern, Switzerland
10 Bern Center for Precision Medicine, University of Bern, 3008 Bern, Switzerland
* Correspondence: leonore.kuechler@unibe.ch (L.K.); simone.debrot@unibe.ch (S.d.B.)

Simple Summary: In canine urothelial carcinoma, the *BRAF* gene is frequently mutated (V595E). To detect this mutation, urine or tissue samples are currently tested by PCR. Recent advances in digital pathology and the power of artificial intelligence (AI) have opened up new possibilities for the detection of genetic alterations through AI histology. This new approach offers a wide range of new opportunities in the field of diagnostic and predictive tumour marker detection. The aim of this study was to test the efficacy of AI histology to predict the presence of the *BRAF* mutation in canine bladder carcinomas and to assess its intratumoral heterogeneity. This is the first study to utilise AI histology to predict *BRAF* mutational status in canine urothelial cell carcinomas.

Abstract: In dogs, the *BRAF* mutation (V595E) is common in bladder and prostate cancer and represents a specific diagnostic marker. Recent advantages in artificial intelligence (AI) offer new opportunities in the field of tumour marker detection. While AI histology studies have been conducted in humans to detect *BRAF* mutation in cancer, comparable studies in animals are lacking. In this study, we used commercially available AI histology software to predict *BRAF* mutation in whole slide images (WSI) of bladder urothelial carcinomas (UC) stained with haematoxylin and eosin (HE), based on a training (n = 81) and a validation set (n = 96). Among 96 WSI, 57 showed identical PCR and AI-based *BRAF* predictions, resulting in a sensitivity of 58% and a specificity of 63%. The sensitivity increased substantially to 89% when excluding small or poor-quality tissue sections. Test reliability depended on tumour differentiation ($p < 0.01$), presence of inflammation ($p < 0.01$), slide quality ($p < 0.02$) and sample size ($p < 0.02$). Based on a small subset of cases with available adjacent non-neoplastic urothelium, AI was able to distinguish malignant from benign epithelium. This is the first study to demonstrate the use of AI histology to predict *BRAF* mutation status in canine UC. Despite certain limitations, the results highlight the potential of AI in predicting molecular alterations in routine tissue sections.

Keywords: urothelial carcinoma (UC); *BRAF*; artificial intelligence (AI); histology

Citation: Küchler, L.; Posthaus, C.; Jäger, K.; Guscetti, F.; van der Weyden, L.; von Bomhard, W.; Schmidt, J.M.; Farra, D.; Aupperle-Lellbach, H.; Kehl, A.; et al. Artificial Intelligence to Predict the *BRAF V595E* Mutation in Canine Urinary Bladder Urothelial Carcinomas. *Animals* **2023**, *13*, 2404. https://doi.org/10.3390/ani13152404

Academic Editors: Maureen A. Griffin and William T. N. Culp

Received: 12 June 2023
Revised: 10 July 2023
Accepted: 21 July 2023
Published: 25 July 2023

1. Introduction

Urothelial cell carcinoma (UC) is the most common malignant tumour affecting the canine lower urinary tract [1–6]. Since these tumours are not only highly invasive and metastatic but also typically located at the trigonum of the bladder, treatment options are limited, and the prognosis remains guarded to poor [4,6,7]. Scottish Terriers are at an extraordinarily increased risk for developing UC (>20-fold higher than other breeds), and Shetland Sheepdogs, West Highland White Terriers and other terriers are also known to be predisposed [2]. Other risk factors for the development of UC include female sex and being spayed or neutered [2,3]. The increased risk for certain breeds to develop UC strongly suggests an underlying genetic basis [1,2,4–6,8,9]. In recent years, it has been shown that the V595E mutation in *BRAF*, the canine homolog to human *BRAF* V600E, occurs in up to 87% of canine urinary bladder carcinomas, and known high-risk dog breeds are particularly frequently affected [1,3,10–12]. The *BRAF* gene encodes the BRAF protein, which plays a key role in the MAP kinase/ERK signalling pathway and regulates important cellular functions such as cell growth, differentiation, proliferation, senescence, and apoptosis [13]. In humans, mutations in *BRAF* frequently occur in various tumour types, such as melanoma, thyroid carcinoma, and colorectal carcinoma, and it has been shown that the *BRAF* mutation can show inter- and intratumoral heterogeneity [1,14–17]. Very recently, it has been shown that in addition to the high prevalence of *BRAF* mutation in neoplasia of the lower urinary tract and the prostate of the dog, the *BRAF* V595E variant is frequent in canine papillary oral squamous cell carcinomas [18]. However, it is rarely identified (melanocytoma, peripheral nerve sheath tumour) or absent in other tumour types of dogs [10]. Of note, the *BRAF* mutation is rarely observed in human UC, although UC in dogs and the muscle-invasive form of UC in humans share many histopathological similarities [2,4–8,19–23]. The reasons behind this disparity have not yet been elucidated conclusively. Furthermore, the prognostic relevance of *BRAF* mutations in canine UC and the identification of driver genes in UC without *BRAF* mutations remain to be determined [24].

In dogs, detection of *BRAF* V595E mutation is typically carried out by PCR testing and is primarily used as a diagnostic marker to detect carcinomas of the urinary tract or prostate [25,26]. While PCR testing is considered highly specific, it is important to be aware of false negative PCR results depending on the quality and heterogeneity of the tested urine or tissue [25]. The test result also fails to provide spatial information in heterogeneous tumour tissue and benign adjacent tissue.

To address these limitations, digital pathology offers a promising solution. Computer-assisted analysis of whole slide images (WSI) allows us to efficiently evaluate cancer tissue sections in an objective, quantitative, and reproducible way. Moreover, it can assess complex features like spatial interactions, which are challenging to evaluate through routine light microscopy [27]. Artificial intelligence (AI) has proven to be extremely powerful for extracting and assessing quantitative information from digital histology [28]. Using AI as a tool to detect tissue markers and to classify tumours, e.g., based on morphologic characteristics like tumour grade, level of invasion, and cellular pleomorphism, has resulted in a rapid evolution and expansion of digital pathology [27]. AI can also be applied to detect molecular features, such as the presence of specific genetic alterations and their possible heterogeneity in tissue [29,30].

In veterinary science, the power of AI in pathology and imaging has recently gained a great deal of attention and continues to do so [31–34]. However, only a few animal studies in this field are currently available. In order to test the options of AI to predict specific molecular alterations on routine, HE-stained tissue sections, a specific genetic mutation, and the associated disease needs to be defined first. In the field of canine cancer, the most characterised and most frequently tested somatic mutations are *c-kit* in mast cell tumours and *BRAF* in bladder and prostate cancer [3,11,12,35–37]. The use of AI to predict *c-kit* mutation has been reported recently [38]. Considering the lack of any AI histology studies on *BRAF* in dogs and with the availability of a specific PCR test for this mutation, we selected this gene for testing the options of AI. In recent years, AI has been

successfully used to predict *BRAF* mutation status with high accuracy in human tumours, such as melanoma, thyroid carcinoma and colorectal carcinoma from radiological scans or WSIs [14,16,39–43]. The present study aimed to test AI histology to predict the presence of the *BRAF* V595E mutation in canine urinary bladder urothelial carcinomas.

2. Materials and Methods

a. Case Selection

The pathology archives of the Institute of Animal Pathology were searched for cases of primary carcinomas of the canine bladder. Additional cases were provided in collaboration with the Institute of Veterinary Pathology in Zurich, Switzerland; Laboklin Bad Kissingen, Germany; Synlab Vet Animal Pathology Munich, Munich, Germany and the Small Animal Clinic Hofheim, Hofheim, Germany. Of 157 dogs, 177 haematoxylin and eosin (HE) stained slides of tumour tissue and/or benign bladder tissue were available for analysis. For eight dogs, two or more WSI were selected per case, as the different slides contained either variable amounts of neoplastic and benign tissue or differed significantly in tumour histomorphology. All slides were scanned using the NanoZoomer S360MD Slide scanner system (Hamamatsu Photonics, Shizuoka, Japan). Signalment data were obtained and included breed, sex, neutering status, and age. All cases were reviewed and classified by a single pathologist as 'highly valuable' (defined as transmural bladder sections with well-preserved histomorphology), 'standard' (non-transmural section with well-preserved histomorphology), or 'poor' (small sample size or ill-preserved tissue). Additionally, the tumours were classified according to their morphology ('conventional UC': predominantly urothelial differentiation; versus 'non-conventional': urothelial differentiation minor or absent); invasion ('non-invasive': tumour borders little or non-invasive; versus 'invasive': clear tumour infiltration into lamina propria or lamina muscularis), and associated inflammation ('inflammatory': moderate to large numbers of leukocytes infiltrate the tumour parenchyma focally, multifocally, or diffusely; versus 'non-inflammatory': none or low numbers of infiltrating leukocytes).

b. PCR

Extraction of DNA from the paraffin-embedded formalin-fixed (FFPE) samples was performed using the QIAamp® DNA FFPE Tissue Kit (Qiagen, Hilden, Germany) according to the manufacturer's instructions. Isolated DNA was examined for the presence of the *BRAF* mutation c.1784T > A by digital droplet polymerase chain reaction (ddPCR) using a mutation-specific TaqMan® assay as described by Mochizuki et al. [25]. Analysis was performed using DropletReader (Bio-Rad, Feldkirchen, Germany) and QuantaSoft™ Software (Bio-Rad, Feldkirchen, Germany).

c. AI Histology

For the digital histological analysis, commercially available software was used (Visiopharm 2022.11, Hørsholm, Denmark). All histological analyses, as well as deep learning training, were based on the WSI of HE stained tissue sections on glass slides. The slides were assessed in the following workflow using three different automated analytic programs designed specifically for this project (Figure 1).

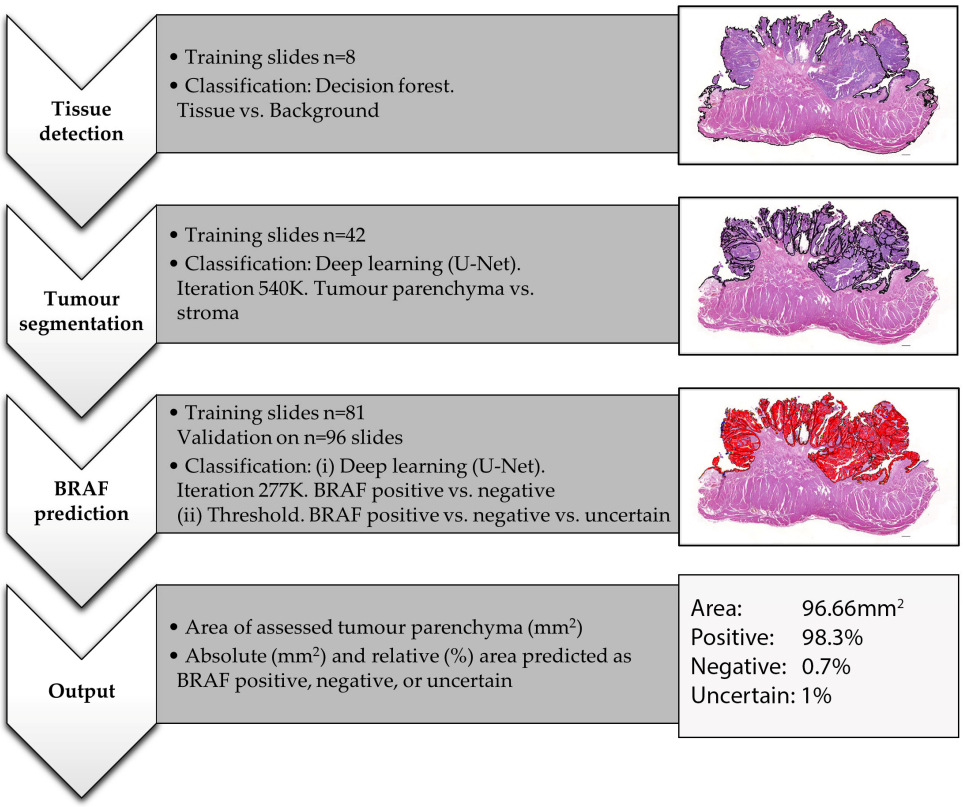

Figure 1. Workflow of the performed AI training and analysis for *BRAF* mutation prediction on WSI of HE-stained canine urothelial carcinomas. The images represent a case of bladder UC from an 11-year-old female neutered Jack Russell Terrier with positive BRAF PCR. This figure shows the output of threshold 0.6.

(i) Tissue detection.

Based on training slides (n = 8), decision forest classification at magnification 0.5× was used to detect any HE-stained tissue on the slide and to outline the generated tissue label as a region of interest (ROI). Where needed, manual corrections were performed, which were minor in the majority of cases.

(ii) Tissue and tumour segmentation.

Based on training slides (n = 42) and 540 K iterations, deep learning (U-Net) classification at magnification 3× was used to separate tumour parenchyma from the stroma and non-tumour tissue and to outline the generated parenchyma label as ROI. On all slides, manual corrections were performed where needed, which were minor in non-invasive and major in highly invasive or poor-quality tumours. The area of this ROI was then measured in an automated way to evaluate the sample size.

(iii) *BRAF* mutation prediction

The case selection was first divided into a training and a validation set (Table 1). Assuming that the 'high quality' cases would be most valuable for AI training, these samples were preferred for the training set. Otherwise, the division into the two groups was performed randomly. The training set included cases of bladder UC from 73 dogs (81 slides) from 30 different breeds. The validation set consisted of 84 cases (96 slides) of bladder UC from 34 different breeds. Of these validation cases, 34 were classified as high quality, 19 as standard, and 43 as poor. Fifty were classified as predominantly urothelial and 46 as minor or absent-urothelial differentiated. Thirty-four tumours were categorised as infiltrative, 23 as little or non-infiltrative, and for 39 tumours, no classification could be achieved due to a small sample size or poor quality.

Table 1. Overview of the n = 177 WSI used for AI training and analysis. Abbreviations: conv.: conventional (urothelial); NA: not assessable; ROI: Region of interest (i.e., tissue area used for training or analysis).

	Training Set			Validation Set		
No. of slides		81			96	
PCR	positive	negative		positive	Negative	
	37	44		69	27	
Mean ROI	256 ± 135 mm^2 (entire tissue section)			14 ± 3 mm^2 (epithelium only)		
Quality	high	standard	poor	high	standard	poor
	80	1	0	34	19	43
PCR positive	37	0	0	27	15	27
PCR negative	43	1	0	7	4	16
Differentiation	conv.	non-conv.		conv.	non-conv.	
	71	10		50	46	
PCR positive	36	1		40	29	
PCR negative	35	9		10	17	
Invasion	present	absent	NA	present	Absent	NA
	44	36	1	34	23	39
PCR positive	22	15	0	23	19	27
PCR negative	22	21	1	11	4	12
Inflammation	present	absent	NA	present	Absent	NA
	32	49	0	39	56	1
PCR positive	15	22	0	28	40	1
PCR negative	17	27	0	11	16	0

Based on the 81 training slides and 277 K iterations, deep learning (U-Net) classification at magnification 2× was used to predict *BRAF* mutation as either positive or negative. For the training, the entire tissue section was either labelled as positive or negative, depending on the corresponding PCR result. Based on the generated deep learning feature, we then used three different threshold classifications to predict *BRAF* mutation for each pixel in the previously defined tumour parenchyma ROI of validation cases:

(1) Threshold 0.6: positive (≥0.6 probability), negative (≥0.6 probability) or uncertain (<0.6 positive and <0.6 negative);
(2) Threshold 0.7: positive (≥0.7 probability), negative (≥0.7 probability) or uncertain (<0.7 positive and <0.7 negative);
(3) Threshold 0.5: positive (≥0.5 probability) or negative (≥0.5 probability).

The analytic programs generated the following outputs for the validation set: area of assessed tumour parenchyma (mm^2) (multiple tissue fragments were summarised); absolute (mm^2) and relative (%) tumour area predicted as *BRAF* positive, negative and, for thresholds 0.7 and 0.6, uncertain (Figure 1). The final AI-*BRAF* prediction was defined as either positive or negative based on the predominant label (e.g., tumour labelled as 47% *BRAF* positive, 45% *BRAF* negative, 8% uncertain is overall predicted as AI-*BRAF* positive). In order to assess whether the AI-*BRAF* prediction was correct, the corresponding PCR result available for each tumour was used as a gold standard and compared with the AI values. If the AI-*BRAF* assessment and the corresponding PCR result did not match, the case was interpreted to be incorrect by AI-based *BRAF* prediction.

Once labelled, the slides were reviewed in order to detect any correlation between AI-based *BRAF* prediction and histomorphology.

In 15 cases, benign urothelium adjacent to the tumour was present on the WSI. For these cases, we subdivided the slide into benign only and tumour only and performed the AI analyses for these two areas separately.

d. Statistical Analysis

A two-sample *t*-test was performed to compare the sample size (i.e., assessed tissue area defined as the region of interest) with the correct or incorrect prediction of the AI tool.

The chi-square test was used to test for associations between AI-based *BRAF* prediction and quality (poor, standard, excellent), morphology (conventional urothelial versus non-conventional differentiation), inflammation (present or absent), and invasion (present or absent). For both tests, p values < 0.05 were considered to indicate a statistically significant difference. Statistical analysis was performed with NCSS 2022 (v22.04, Kaysville, UT, USA).

3. Results

Histologic analysis of the validation set confirmed the presence of well-preserved (standard and high quality) tissue in 53 out of 96 (55%) bladder UC tissue slides (Table 1) examined. For a large proportion (34/53; 64%), tissue samples consisted of transmural bladder sections, which were defined as high-quality histology sections. The remaining slides were of reduced tissue quality, with the presence of tissue artefacts (most commonly tissue folds, suboptimal tissue fixation) or a very small sample size of a few mm^2 or less. Tumour differentiation was conventional urothelial in approximately half of the cases (50/96), whereas the other half were defined as non-conventional UC based on histomorphology. Invasion into underlying lamina propria or tunica muscularis was evident in the majority (34/57; 60%) of assessable tumour slides, whereas the remaining cases were non- or poorly invasive with primarily pushing and smooth tumour borders. Stromal inflammation was present in 39 out of 95 (41%) assessable cases, characterised by mild to moderate, predominantly lymphoplasmacytic infiltrates.

After the initial histomorphological examination, the designed AI tool was used to predict *BRAF* mutation on all available (n = 96) WSI. The PCR testing identified the majority of cases as positive (69/96, 72%, versus 27/96, 28%). The three different (0.5, 0.6 and 0.7 deep learning classifier probability) threshold analyses for mutation prediction yielded different tissue areas predicted to be mutation positive, negative, or uncertain (for thresholds of 0.6 and 0.7). However, the final prediction of the entire WSI remained the same when running these three analytical programs. Thus, the three threshold analyses identically predicted the respective tumours as mutation-positive or negative overall, even though the relative positive vs. negative areas differed for each threshold.

When comparing the AI-based *BRAF* prediction of each WSI with the corresponding PCR result, 57 out of 96 (59%) showed identical results, which was interpreted as the correct prediction (Table 2). False positive predictions were observed in approximately one-third of the negative tested cases (10/27; 37%), while false negative predictions occurred in 42% of the positive cases (29/69). Overall, the specificity (SP) of the AI mutation prediction was 63%, and the sensitivity (SE) was 58%.

Table 2. Comparison of the AI-based *BRAF* prediction of each case with the corresponding PCR result.

AI Prediction	PCR Result Positive	PCR Result Negative	Total Number of Cases
BRAF positive	40	10	50
BRAF negative	29	17	46
Total no. cases	69	27	96

The sensitivity increased significantly when the WSI of reduced quality (i.e., ill-preserved histomorphology or small sample size) were excluded (Table 3 and Supplemental Table S1). The best AI prediction performance was achieved for the high-quality samples (n = 34) with a sensitivity of 89% and specificity of 43%. Sensitivity was reduced to 47% and 33% for standard (n = 19) and poor quality (n = 43) WSI, respectively. In contrast, specificity was higher in WSI of reduced quality, ranging from 69% (poor quality) to 75% (standard sample).

Table 3. Comparison of AI-based *BRAF* mutation prediction with confirmed PCR result based on specific histomorphological features. Shown in brackets is the number of cases where the PCR result matched the AI result. Abbreviations: SE: sensitivity; SP: specificity; stand: standard.

AI Prediction	**No. Cases**		
Quality	High	Stand	Poor
BRAF positive	28 (24)	8 (7)	14 (9)
BRAF negative	6 (3)	11 (3)	29 (11)
	SE [%]: 89	SE [%]: 47	SE [%]: 33
	SP [%]: 43	SP [%]: 75	SP [%]: 69
Urothelial differentiation	Present		Absent
BRAF positive	42 (34)		8 (6)
BRAF negative	8 (2)		38 (15)
	SE [%]: 85		SE [%]: 21
	SP [%]: 20		SP [%]: 88
Invasive tumour front	Present		Absent
BRAF positive	10 (8)		19 (16)
BRAF negative	24 (9)		4 (1)
	SE [%]: 35		SE [%]:84
	SP [%]: 82		SP [%]: 25
Inflammation	Present		Absent
BRAF positive	11 (8)		39 (32)
BRAF negative	28 (8)		17 (9)
	SE [%]: 29		SE [%]: 80
	SP [%]: 73		SP [%]: 56

When comparing the performance of the AI prediction with tumour histomorphology, the level of urothelial differentiation was highly relevant ($p < 0.01$) (Table 4). WSI of conventional UC with evident urothelial morphology ($n = 50$) had a high sensitivity of 85%, which dropped to 21% in cases with ill-defined or absent urothelial differentiation ($n = 46$). The opposite was true when comparing the specificity, which was significantly higher in non-conventional (88%) compared to conventional (20%) UC. With regard to the level of tumour invasiveness, the AI prediction was highly sensitive (SE 84%) for non-invasive tumours and highly specific (SP 82%) for invasive UC. Sensitivity and specificity were, however, low for invasive ($n = 34$; SE 35%) and non-invasive ($n = 23$; SP 25%) tumours, respectively. The remaining cases were not assessable for the level of invasion due to their small size or reduced quality. Considering tumour inflammation, the AI test sensitivity was low (SE 29%) for inflamed UC ($n = 39$), whereas the opposite was true for those with associated inflammation ($n = 56$) (SE 80%). The specificity was higher (SP = 73%) for inflamed UC when compared to non-inflamed tumours (SP 56%). In one case, the level of inflammation was not assessable due to poor quality.

Table 4. Assessing the AI tool's reliability for correct *BRAF* mutation prediction based on specific features across different sample cohorts. A Chi-square test was performed for categorical data (urothelial differentiation, inflammation, slide quality, invasive growth, and mutation status) and a two-sided *t*-test for continuous data (sample size). *p* values of <0.05 were considered significant (in bold).

Feature	**All Samples**	**Standard and High-Quality Samples Only**	**High-Quality Samples Only**
Urothelial differentiation	**<0.01**	>0.1	>0.9
Inflammation	**<0.01**	**<0.03**	>0.7
Slide quality	**<0.02**	NA	NA
Sample size (ROI)	**<0.02**	>0.08	>0.3
Invasive growth	>0.08	>0.3	>0.2
Mutation status (PCR)	>0.6	>0.1	**<0.02**

Independent of the histomorphological quality, sample size played a significant role in the AI test reliability ($p < 0.02$) (Table 4). This effect was most evident and beneficial when investigating *BRAF* mutation-positive cases where a larger sample size correlated with a higher level of correct prediction ($p < 0.003$) (Supplemental Table S2). In contrast, *BRAF*-negative tumours had a tendency for false positive AI predictions with increasing sample size ($p > 0.3$). Test reliability also depended significantly on tumour differentiation ($p < 0.01$), presence of inflammation ($p < 0.01$), slide quality ($p < 0.02$) and sample size ($p < 0.02$).

In addition to the relative and overall *BRAF* mutation prediction, the AI assessment enabled the visualisation of the intratumour mutation heterogeneity, which allowed the investigation of the correlation of *BRAF* mutation with tumour histomorphology. As seen above for the different tumour classes, positive *BRAF* mutation prediction was associated with tumour regions characterised by papillary growth, a smooth and pushing rather than invasive tumour front, and urothelial differentiation (Figures 2 and 3). Histomorphological characteristics which tended to correlate with a negative *BRAF* mutation prediction were the following: solid tumour growth or divergent non-urothelial differentiation, invasive growth, pronounced tumour inflammation, and poor tissue quality, including artefacts due to squeezing, inadequate preservation, and tears (Figure 3). Tumour areas predicted to be uncertain if the mutation is present or absent were commonly observed at the interface of areas predicted as positive and negative and frequently showed a variety of different features of both the aforementioned groups.

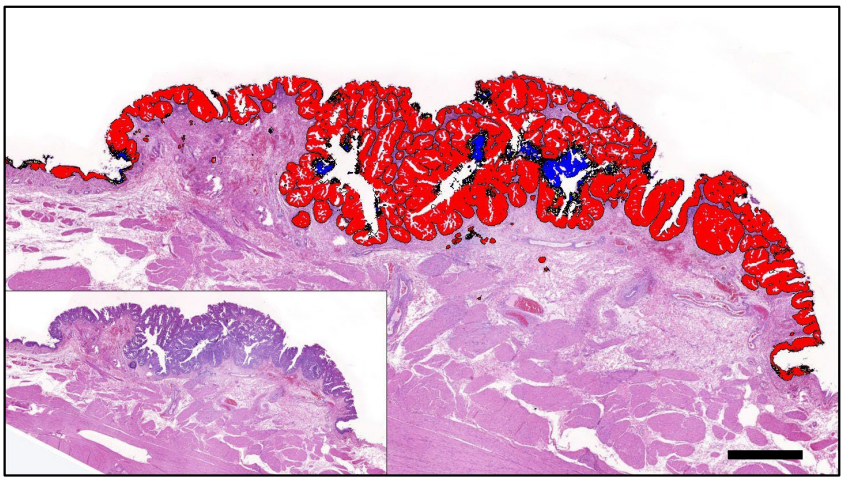

Figure 2. A papillary poorly invasive conventional urothelial carcinoma of a 9-year-old female neutered Scottish Terrier positive for *BRAF* mutation by PCR that was accurately predicted by AI histology. Labelling: red: *BRAF* positive; blue: *BRAF* negative; yellow: uncertain. Threshold classification 0.6. Bar indicates 1 mm.

In addition to the direct correlation of AI-based *BRAF* mutation prediction and tumour histomorphology, the spatial visualisation of mutation prediction was also valuable for the comparative investigation of benign and neoplastic urothelium. For $n = 15$ WSI of the validation set, benign urothelium adjacent to the tumour was available. All but one case was PCR tested mutation positive. The majority (11/14; 79%) of these cases were correctly predicted to bear the mutation based on AI. In six of these PCR-confirmed and AI-predicted positive cases, AI classified benign urothelium as mutation-negative (Figure 4). One such case represented a conventional papillary UC from a Scottish Terrier, where the AI prediction correctly labelled the tumour as mutation-positive and furthermore classified small foci of dysplasia in the adjacent urothelium as positive, while morphologically unremarkable benign urothelium remained negative (Figure 3). The interface of the mutation-positive dysplastic foci and the mutation-negative benign urothelium was labelled as *BRAF*-uncertain. The ability of the AI tool to distinguish malignant from benign

urothelium was confirmed in another case of *BRAF*-mutated UC of a Flat Coated Retriever, where the positive prediction was limited to neoplastic growth (Figure 5).

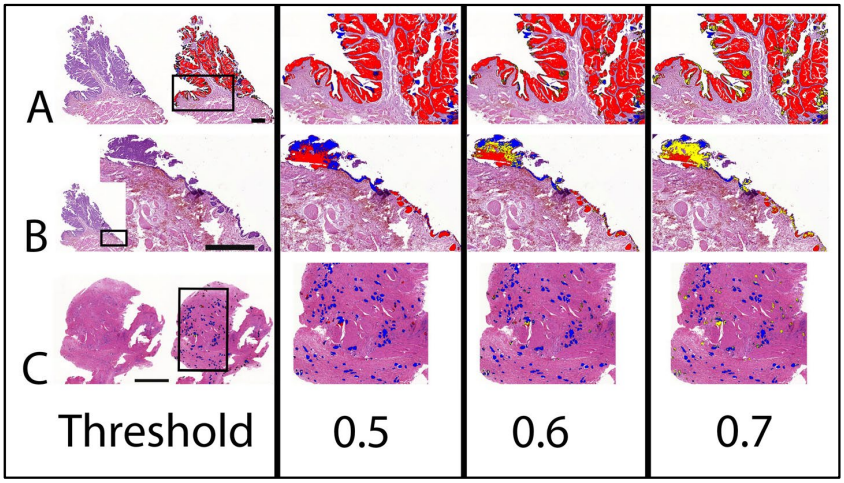

Figure 3. AI prediction of *BRAF* mutation on two cases of UC with different mutation status as confirmed by PCR. The labelling is indicated separately for the three different threshold classifications (0.5 to 0.7). Note that *BRAF* mutation negative labelling is changing to an uncertain label with an increasing threshold. (**A**) Non-invasive papillary UC with predominant positive labelling correctly predicted as mutation positive. Bar indicates 1 mm. (**B**) Adjacent benign tissue of (**A**). Bar indicates 0.5 mm. Benign flat urothelium is labelled negative, whereas Brunn nests are labelled positive. (**C**) Transmural highly invasive UC with predominant negative labelling correctly predicted as mutation negative. Bar indicates 1 mm. Labelling: red: *BRAF* positive; blue: *BRAF* negative; yellow: uncertain.

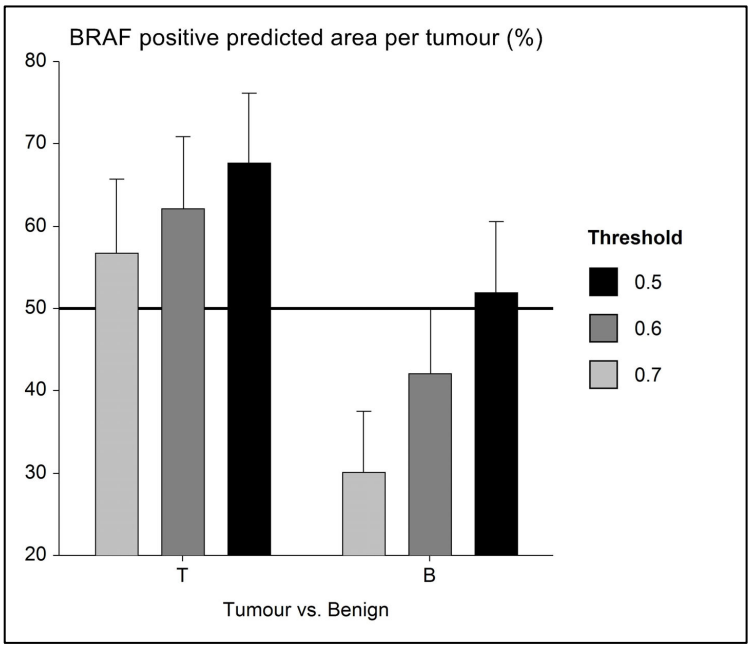

Figure 4. Error bar chart with columns representing mean group values and an indication of the standard error of the mean (SEM). In a small series (n = 14) of *BRAF*-mutated UC with adjacent benign urothelium, the level of mutation prediction (indicated as a percentage of *BRAF* positive labelling) differs, and AI is able to distinguish between tumour (*BRAF* positive) and benign (presumably *BRAF* negative) tissue. As a mean, benign tissue is correctly labelled as mutation negative (i.e., <50% BRAF positive) when using 0.6 and 0.7 AI threshold classifiers.

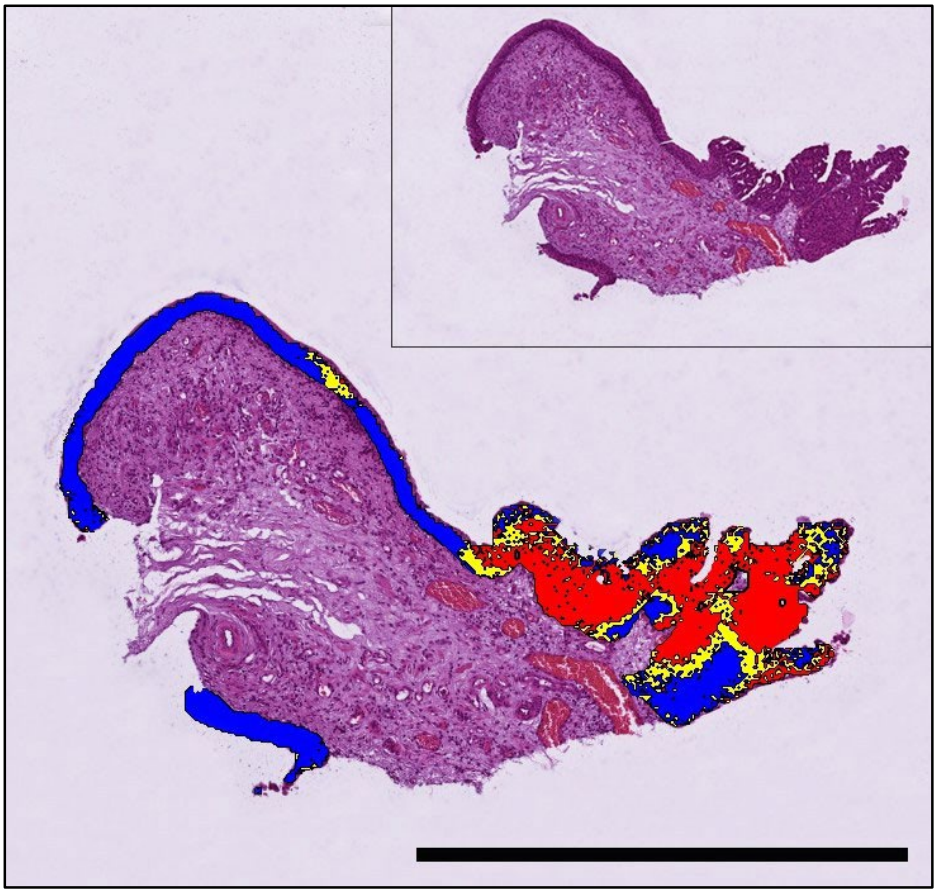

Figure 5. A papillary urothelial carcinoma of a 9-year-old Flat-coated Retriever that tested positive for *BRAF* mutation by PCR and was correctly predicted by AI histology. The mutation is predicted to be present in the neoplastic growth, whereas adjacent benign urothelium is labelled mutation-negative (threshold classification 0.6). Labelling: red: *BRAF* positive; blue: *BRAF* negative; yellow: uncertain. Bar indicates 1 mm.

4. Discussion

Although AI and machine learning (ML) offer various promising advantages when compared to the routine histopathological examination of tumour tissue by a single pathologist, there are a number of significant challenges to their implementation in practice. In contrast to the defined and reproducible histomorphological parameters (e.g., level of invasion, cell or nuclear size, mitotic activity), the features which are relevant for AI-based decisions often remain unknown. This can pose a challenge to the interpretation and reproduction of results generated by AI. In the context of histology, it is key not to rely solely on AI results, but to consider them together with histomorphology. It is well known that the performance of AI models increases with the size and diversity of the training set. However, on occasions, the available dataset may only be relatively small, especially when dealing with rare tumours and/or subtypes. Another crucial factor is the division of the collection of WSIs into a training set and a validation set, and a large discrepancy between these two sets (such as an imbalance in the distribution of histological subtypes) can lead to poor results. In addition to the level of tissue section preparation, the quality of HE staining (staining depth, uniformity, and presence of dye impurities) and the imaging scan of the section are also factors affecting AI training and interpretation [44–46]. Therefore, the selection of one or multiple different slide scanners, scan resolution, and staining quality is relevant for AI-based histology studies [42,47–49]. For the present study, the AI tool was designed based on the conditions of a single institution (Institute of Animal Pathology, University of Bern), with one specific scanner (NanoZoomer S360MD, Hamamatsu Pho-

tonics), a defined (20×) scan resolution, and tissue slides with highly variable HE staining, histomorphology, sample size and quality. Studies using AI histology based on a single institution and the use of a single scanner have already been described in comparable human studies [50]. With respect to the prediction of the BRAF mutation in human cancer, various AI approaches have been described in the literature, and each has its strengths and weaknesses [14,17,43].

In our study, sample size, i.e., the area of neoplastic urothelium on the corresponding WSI, was confirmed to be important for the AI test performance. Large samples of mutation PCR-positive UC were often correctly predicted as such, whereas the opposite was true for mutation-negative cases with large sizes. When comparing the mean size of PCR BRAF-positive UC with their negative counterpart, it was apparent that mutated tumours were approximately twice as big in our validation set (mean *BRAF* mutation-positive: 16 mm^2 versus mean *BRAF* negative: 9 mm^2; $p > 0.1$). A possible explanation for the larger average size of *BRAF*-mutated tumours is a sampling bias. Alternatively, if this correlation is true that BRAF mutated tumours tend to be larger at the time they are biopsied, then their frequent papillary and poorly invasive growth most likely explains the larger size when compared to flat UC [2]. Being aware that sample size affects AI prediction, training sets need to be standardised for this criterium to increase the reliability of this or any other AI test. This was not done for this study and therefore represents a limitation, which needs to be addressed for future AI studies. A minor (not statistically significant) difference in sample size was indeed observed in the training set with larger tissue sections for mutated (261 mm^2) compared to non-mutated UC (251 mm^2). However, it is important to note that the sample size of training and validation slides cannot be compared directly as their tissue samples were defined differently. The sample of the training slide was defined as all available tissue, i.e., tumour parenchyma as well as stroma and surrounding non-neoplastic tissue, whereas the tissue sample for *BRAF* prediction was restricted to the tumour parenchyma of the UC. When comparing sample size with slide quality, it was evident that a larger sample size was associated with higher quality (with 31.93 mm^2 for high quality, 6.57 mm^2 for standard quality, and 2.37 mm^2 for poor quality) as sample size was a criterion to define quality. We therefore, concluded that the AI possibly used the size of the tumour as a criterion for *BRAF* prediction, which would also explain why tumours of smaller size, like those of poor quality, were often misinterpreted by AI as negative when actually PCR BRAF positive while large PCR BRAF negative UC was frequently misinterpreted as positive. This correlation was to be expected since large specimens were usually transmural sections and therefore defined as high quality. Small samples were often squeezed, difficult to orient and/or had other artefacts that negatively affected the assessment and were therefore classified as poor quality. For future studies, it would be conceivable that training labels should be of similar size, independent of the size of the tissue section on the WSI. For this purpose, one or several regions with a specific size and shape (e.g., a square of 1 mm^2) could be defined, and training labels created only in these regions.

Our study found that the level of tumour inflammation markedly affected the sensitivity of the AI-based *BRAF* prediction, which was low for inflamed UC and high in those without associated inflammation. In contrast, the specificity was higher in inflamed than non-inflamed UC. There was no considerable difference in the ratio of inflamed to non-inflamed UC when comparing the training group with the validation group or when comparing different mutation statuses. However, in contrast to the high quality of the UC within the training set, the inflamed UC in the validation set were also often of poor quality (21/39), which could explain the poor sensitivity of the AI-based *BRAF* prediction for this category.

Another factor we identified as being critical determinate for the accuracy of the AI test reliability was the level of urothelial differentiation. For UC with evident urothelial morphology (conventional UC), the mutation was detected by AI with a high level of sensitivity. However, the rate of false positives was high for these tumours. For UC with

only subtle or absent urothelial morphology (non-conventional UC), the AI prediction was highly specific for the mutation-negative cases; however, the rate of false negative cases was high. The large discrepancy between sensitivity and specificity for non-conventional UC cases may have been influenced by the imbalance in the training set: 71/81 cases in the training showed conventional urothelial morphology and only 10 were of divergent differentiation. In addition, none of the latter were PCR negative for BRAF. Thus, the training set only included one non-conventional UC with positive BRAF PCR, which could explain the poor sensitivity of our AI tool for this category.

Similar to the extent of urothelial differentiation, the level of tumour invasiveness was closely associated with the AI test reliability. UC with a clearly invasive tumour border tended to be predicted as mutation negative on AI, which resulted in a high specificity but low sensitivity, whereas the non-invasive tumours had a high sensitivity and low specificity. The reason for the large discrepancy between the sensitivity and specificity of invasive and non-invasive UC cases was not obvious. However, 39 of 96 cases could not be assessed for their level of invasion due to sample size and/or quality. Thus, there were far fewer cases available for assessment of invasion than for other tumour characteristics, which limited the interpretation of this factor.

In human cancers with frequent (V600E) *BRAF* mutation, it is widely recognised that intratumoral heterogeneity exists; however, intratumoral *BRAF* mutation heterogeneity has not yet been described in canine cancer. In this study, we show that *BRAF* mutation prediction correlated with defined morphologic features. For example, areas with papillary growth, smooth and pushing tumour fronts and urothelial differentiation were often predicted as being *BRAF V595* positive (i.e., BRAF mutated). In contrast, areas with a more solid tumour growth pattern, divergent urothelial differentiation and invasive growth were often predicted as mutation negative. Pronounced tumour inflammation also led to *BRAF*-negative prediction. Additionally, artefacts like squeezing or poor tissue preservation were usually also interpreted to lack a *BRAF* mutation. Locations with 'uncertain prediction' were usually identified at the interface between positive and negative tumour areas. Thus, genetic heterogeneity within the tumour needs to be factored in when making a diagnosis, especially if the treatment involves therapeutic strategies that depend on the presence or absence of *BRAF* mutation. Indeed, studies have shown that *BRAF* mutation status influences the treatment response in human cancers [51,52], and there is evidence for a different therapeutic response when comparing *BRAF* mutated vs. non-mutated canine cancers [35,53,54].

The *BRAF* mutation is found in malignant urothelium and not benign bladder or in urine from healthy dogs [10,11,55], making it a highly-specific marker for UC, with additional advantages of being non-invasive and inexpensive if performed on urine. In cases where UC is suspected and the *BRAF* mutation is not detected by PCR in urine, a bladder biopsy is needed to confirm or exclude UC. Not uncommonly, histologic evaluation can be difficult when dealing with early forms of UC or only small endoscopic biopsies. In this situation, the pathologist needs to have a high level of experience to reach a definite diagnosis, and the risk of missing small cancerous lesions exists. The power of AI for supporting the pathologist in detecting early and small cancer foci has been demonstrated for bladder and other cancers in humans [56–58]. Even though limited to a small series (n = 14) of *BRAF*-mutated UC, the present study confirms that AI was able to distinguish between malignant and adjacent benign urothelium in six cases. Considering that the separation of benign and malignant tissue was not the main aim of this study, the training was not specifically set up to perform this task. Nevertheless, AI has shown that benign urothelium more closely resembles *BRAF* mutation negative rather than positive tumours, as benign regions were labelled as such in the present study. With optimised training and based on the promising results from human studies, it can be expected that AI will be able to reliably differentiate benign urothelium from neoplastic bladder tissue in dogs [59,60].

5. Conclusions

This is the first study to demonstrate the use of AI histology to predict *BRAF* mutation status in canine UC. Despite certain limitations, which we were able to define, the results highlight the potential of AI in predicting molecular alterations in routine tissue sections. Important potential confounding factors are sample size and quality, as well as tumour histomorphology. Once optimised for these features, AI is able to reliably predict *BRAF* mutation, detect intratumoral mutation heterogeneity and differentiate between malignant and benign urothelium.

Supplementary Materials: The following supporting information can be downloaded at: https://www.mdpi.com/article/10.3390/ani13152404/s1, Table S1: Comparison of AI-based BRAF mutation prediction with confirmed PCR result based on sample quality and specific histomorphological features; Table S2: Extension of Table 4.

Author Contributions: Conceptualisation, methodology, digital pathology, validation: L.K., S.d.B., C.P., S.R.; PCR: A.K.; Analysis: L.K., S.d.B., C.P., D.F., A.K., L.v.d.W., W.v.B.; Writing-original draft preparation: L.K.; Writing-review and editing: S.d.B., W.v.B., H.A.-L., J.M.S., D.F., F.G., K.J., L.v.d.W., S.R.; Supervision: S.d.B., S.R. All authors have read and agreed to the published version of the manuscript.

Funding: Funding for this study was provided by institutional grants of the University of Bern (Promotion of Early Career Researchers and Gender Equality; Bern University Research Foundation; and the Specialization Commission of the Vetsuisse Faculty) and the Albert Heim Foundation (grant number 148).

Informed Consent Statement: Not applicable.

Data Availability Statement: The data that support the findings of this study are available from the corresponding authors, L.K. and S.d.B., upon reasonable request.

Acknowledgments: The authors would like to thank Astrid Chanfon for scanning all tissue slides.

Conflicts of Interest: The authors do declare no conflict of interest. However, Heike Aupperle-Lellbach, Kathrin Jaeger, and Wolf von Bomhard do offer diagnostic pathology services.

References

1. Jung, H.; Bae, K.; Lee, J.Y.; Kim, J.H.; Han, H.J.; Yoon, H.Y.; Yoon, K.A. Establishment of canine transitional cell carcinoma cell lines harboring BRAF V595E mutation as a therapeutic target. *Int. J. Mol. Sci.* **2021**, *22*, 9151. [CrossRef]
2. De Brot, S.; Robinson, B.D.; Scase, T.; Grau-Roma, L.; Wilkinson, E.; Boorjian, S.A.; Gardner, D.; Mongan, N.P. The dog as an animal model for bladder and urethral urothelial carcinoma: Comparative epidemiology and histology. *Oncol. Lett.* **2018**, *16*, 1641–1649. [CrossRef] [PubMed]
3. Grassinger, J.M.; Merz, S.; Aupperle-Lellbach, H.; Erhard, H.; Klopfleisch, R. Correlation of BRAF variant V595E, breed, histological grade and cyclooxygenase-2 expression in canine transitional cell carcinomas. *Vet. Sci.* **2019**, *6*, 31. [CrossRef] [PubMed]
4. Knapp, D.W.; Dhawan, D.; Ramos-Vara, J.A.; Ratliff, T.L.; Cresswell, G.M.; Utturkar, S.; Sommer, B.C.; Fulkerson, C.M.; Hahn, N.M. Naturally-Occurring Invasive Urothelial Carcinoma in Dogs, a Unique Model to Drive Advances in Managing Muscle Invasive Bladder Cancer in Humans. *Front. Oncol.* **2020**, *9*, 1493. [CrossRef]
5. De Brot, S.; Grau-Roma, L.; Stirling-Stainsby, C.; Dettwiler, M.; Guscetti, F.; Meier, D.; Scase, T.; Robinson, B.D.; Gardner, D.; Mongan, N.P. A Fibromyxoid Stromal Response is Associated with Muscle Invasion in Canine Urothelial Carcinoma. *J. Comp. Pathol.* **2019**, *169*, 35–46. [CrossRef] [PubMed]
6. Blackwell, W. *Tumors in Domestic Animals*, 5th ed.; John Wiley & Sons: Hoboken, NJ, USA, 2016.
7. Norris, A.M.; Laing, E.J.; Valli, V.E.O.; Withrow, S.J.; Macy, D.W.; Ogilvie, G.K.; Tomlinson, J.; McCaw, D.; Pidgeon, G.; Jacobs, R.M. Canine Bladder and Urethral Tumors: A Retrospective Study of 115 Cases (1980–1985). *J. Vet. Intern. Med.* **1992**, *6*, 145–153. [CrossRef]
8. Fulkerson, C.M.; Knapp, D.W. Management of transitional cell carcinoma of the urinary bladder in dogs: A review. *Vet. J.* **2015**, *205*, 217–225. [CrossRef]
9. Fulkerson, C.M.; Dhawan, D.; Ratliff, T.L.; Hahn, N.M.; Knapp, D.W. Naturally Occurring Canine Invasive Urinary Bladder Cancer: A Complementary Animal Model to Improve the Success Rate in Human Clinical Trials of New Cancer Drugs. *Int. J. Genom.* **2017**, *2017*, 6589529. [CrossRef]
10. Mochizuki, H.; Kennedy, K.; Shapiro, S.G.; Breen, M.B. BRAF mutations in canine cancers. *PLoS ONE* **2015**, *10*, e0129534. [CrossRef]

11. Ostrander, E.; Decker, B.; Parker, H.G.; Dhawan, D.; Kwon, E.M.; Karlins, E.; Davis, B.; Ramos-vara, J.A.; Bonney, P.L.; McNiel, E.A.; et al. Homologous Mutation to Human BRAF V600E is Common in Naturally Occurring Canine Bladder Cancer—Evidence for a Relevant Model System and Urine-based Diagnostic Test. *Mol. Cancer Res.* **2012**, *17*, 1310–1314. [CrossRef]
12. Mochizuki, H.; Breen, M. Comparative aspects of BRAF mutations in canine cancers. *Vet. Sci.* **2015**, *2*, 231–245. [CrossRef] [PubMed]
13. Dhillon, A.S.; Hagan, S.; Rath, O.; Kolch, W. MAP kinase signalling pathways in cancer. *Oncogene* **2007**, *26*, 3279–3290. [CrossRef] [PubMed]
14. Anand, D.; Yashashwi, K.; Kumar, N.; Rane, S.; Gann, P.H.; Sethi, A. Weakly supervised learning on unannotated H&E-stained slides predicts BRAF mutation in thyroid cancer with high accuracy. *J. Pathol.* **2021**, *255*, 232–242. [CrossRef] [PubMed]
15. Xing, M.; Alzahrani, A.S.; Carson, K.A.; Shong, Y.K.; Kim, T.Y.; Viola, D.; Robenshtok, E.; Fagin, J.A.; Puxeddu, E.; Fugazzola, L.; et al. Association Between BRAF V600E Mutation and Recurrence of Papillary Thyroid Cancer. *J. Clin. Oncol.* **2015**, *33*, 42–50. [CrossRef]
16. Yoon, J.; Lee, E.; Koo, J.S.; Yoon, J.H.; Nam, K.H.; Lee, J.; Jo, Y.S.; Moon, H.J.; Park, V.Y.; Kwak, J.Y. Artificial intelligence to predict the BRAFV600E mutation in patients with thyroid cancer. *PLoS ONE* **2020**, *15*, e0242806. [CrossRef]
17. Ito, T.; Tanaka, Y.; Murata, M.; Kaku-Ito, Y.; Furue, K.; Furue, M. BRAF Heterogeneity in Melanoma. *Curr. Treat. Options Oncol.* **2021**, *22*, 20. [CrossRef]
18. Peralta, S.; Webb, S.M.; Katt, W.P.; Grenier, J.K.; Duhamel, G.E. Highly recurrent BRAF p.V595E mutation in canine papillary oral squamous cell carcinoma. *Vet. Comp. Oncol.* **2023**, *21*, 138–144. [CrossRef]
19. Forbes, S.A.; Beare, D.; Bindal, N.; Bamford, S.; Ward, S.; Cole, C.G.; Jia, M.; Kok, C.; Boutselakis, H.; De, T.; et al. High-Resolution Cancer Genetics Using the Catalogue of Somatic Mutations in Cancer. *Curr. Protoc. Hum. Genet.* **2016**, *91*. [CrossRef]
20. Robertson, A.G.; Kim, J.; Al-ahmadie, H.; Bellmunt, J.; Guo, G.; Cherniack, A.D.; Hinoue, T.; Laird, P.W.; Katherine, A.; Akbani, R.; et al. HHS Public Access bladder cancer. *Cell* **2018**, *171*, 540–556. [CrossRef]
21. Iyer, G.; Al-Ahmadie, H.; Schultz, N.; Hanrahan, A.J.; Ostrovnaya, I.; Balar, A.V.; Kim, P.H.; Lin, O.; Weinhold, N.; Sander, C.; et al. Prevalence and co-occurrence of actionable genomic alterations in high-grade bladder cancer. *J. Clin. Oncol.* **2013**, *31*, 3133–3140. [CrossRef]
22. Boulalas, I.; Zaravinos, A.; Delakas, D.; Spandidos, D.A. Mutational analysis of the BRAF gene in transitional cell carcinoma of the bladder. *Int. J. Biol. Markers* **2009**, *24*, 17–21. [CrossRef] [PubMed]
23. Longo, T.; McGinley, K.F.; Freedman, J.A.; Etienne, W.; Wu, Y.; Sibley, A.; Owzar, K.; Gresham, J.; Moy, C.; Szabo, S.; et al. Targeted Exome Sequencing of the Cancer Genome in Patients with Very High-risk Bladder Cancer. *Eur. Urol.* **2016**, *70*, 714–717. [CrossRef] [PubMed]
24. Thomas, R.; Wiley, C.A.; Droste, E.L.; Robertson, J.; Inman, B.A.; Breen, M. Whole exome sequencing analysis of canine urothelial carcinomas without BRAF V595E mutation: Short in-frame deletions in BRAF and MAP2K1 suggest alternative mechanisms for MAPK pathway disruption. *PLoS Genet.* **2023**, *19*, e1010575. [CrossRef] [PubMed]
25. Mochizuki, H.; Shapiro, S.G.; Breen, M. Detection of BRAF mutation in urine DNA as a molecular diagnostic for canine urothelial and prostatic carcinoma. *PLoS ONE* **2015**, *10*, e0144170. [CrossRef]
26. Rasteiro, A.M.; Sá E Lemos, E.; Oliveira, P.A.; Gil da Costa, R.M. Molecular Markers in Urinary Bladder Cancer: Applications for Diagnosis, Prognosis and Therapy. *Vet. Sci.* **2022**, *9*, 107. [CrossRef]
27. Davis, A.S.; Chang, M.Y.; Brune, J.E.; Hallstrand, T.S.; Johnson, B.; Lindhartsen, S.; Hewitt, S.M.; Frevert, C.W. The Use of Quantitative Digital Pathology to Measure Proteoglycan and Glycosaminoglycan Expression and Accumulation in Healthy and Diseased Tissues. *J. Histochem. Cytochem.* **2021**, *69*, 137–155. [CrossRef]
28. Acs, B.; Rantalainen, M.; Hartman, J. Artificial intelligence as the next step towards precision pathology. *J. Intern. Med.* **2020**, *288*, 62–81. [CrossRef]
29. Qu, H.; Zhou, M.; Yan, Z.; Wang, H.; Rustgi, V.K.; Zhang, S.; Gevaert, O.; Metaxas, D.N. Genetic mutation and biological pathway prediction based on whole slide images in breast carcinoma using deep learning. *npj Precis. Oncol.* **2021**, *5*, 87. [CrossRef]
30. Chen, M.; Zhang, B.; Topatana, W.; Cao, J.; Zhu, H.; Juengpanich, S.; Mao, Q.; Yu, H.; Cai, X. Classification and mutation prediction based on histopathology H&E images in liver cancer using deep learning. *npj Precis. Oncol.* **2020**, *4*, 14. [CrossRef]
31. Zuraw, A.; Aeffner, F. Whole-slide imaging, tissue image analysis, and artificial intelligence in veterinary pathology: An updated introduction and review. *Vet. Pathol.* **2022**, *59*, 6–25. [CrossRef]
32. Hespel, A.M.; Zhang, Y.; Basran, P.S. Artificial intelligence 101 for veterinary diagnostic imaging. *Vet. Radiol. Ultrasound* **2022**, *63*, 817–827. [CrossRef] [PubMed]
33. Gardner, J.; O'Leary, M.; Yuan, L. Artificial intelligence in educational assessment: 'Breakthrough? Or buncombe and ballyhoo?'. *J. Comput. Assist. Learn.* **2021**, *37*, 1207–1216. [CrossRef]
34. Lustgarten, J.L.; Zehnder, A.; Shipman, W.; Gancher, E.; Webb, T.L. Veterinary informatics: Forging the future between veterinary medicine, human medicine, and One Health initiatives-a joint paper by the Association for Veterinary Informatics (AVI) and the CTSA One Health Alliance (COHA). *JAMIA Open* **2020**, *3*, 306–317. [CrossRef] [PubMed]
35. Gedon, J.; Kehl, A.; Aupperle-Lellbach, H.; von Bomhard, W.; Schmidt, J.M. BRAF mutation status and its prognostic significance in 79 canine urothelial carcinomas: A retrospective study (2006–2019). *Vet. Comp. Oncol.* **2022**, *20*, 449–457. [CrossRef]
36. Kiupel, M.; Camus, M. Diagnosis and Prognosis of Canine Cutaneous Mast Cell Tumors. *Vet. Clin. N. Am. Small Anim. Pract.* **2019**, *49*, 819–836. [CrossRef]

37. Tamlin, V.S.; Bottema, C.D.K.; Peaston, A.E. Comparative aspects of mast cell neoplasia in animals and the role of KIT in prognosis and treatment. *Vet. Med. Sci.* **2020**, *6*, 3–18. [CrossRef]
38. Bertram, C.A.; Aubreville, M.; Donovan, T.A.; Bartel, A.; Wilm, F.; Marzahl, C.; Assenmacher, C.A.; Becker, K.; Bennett, M.; Corner, S.; et al. Computer-assisted mitotic count using a deep learning-based algorithm improves interobserver reproducibility and accuracy. *Vet. Pathol.* **2022**, *59*, 211–226. [CrossRef]
39. Shmatko, A.; Ghaffari Laleh, N.; Gerstung, M.; Kather, J.N. Artificial intelligence in histopathology: Enhancing cancer research and clinical oncology. *Nat. Cancer* **2022**, *3*, 1026–1038. [CrossRef]
40. Figueroa-Silva, O.; Pastur Romay, L.A.; Viruez Roca, R.D.; Rojas, M.D.S.A.Y.; Suárez-Peñaranda, J.M. Machine Learning Techniques in Predicting BRAF Mutation Status in Cutaneous Melanoma From Clinical and Histopathologic Features. *Appl. Immunohistochem. Mol. Morphol.* **2022**, *30*, 674–680. [CrossRef]
41. Krebs, F.S.; Britschgi, C.; Pradervand, S.; Achermann, R.; Tsantoulis, P.; Haefliger, S.; Wicki, A.; Michielin, O.; Zoete, V. Structure-based prediction of BRAF mutation classes using machine-learning approaches. *Sci. Rep.* **2022**, *12*, 12528. [CrossRef]
42. Kim, R.H.; Nomikou, S.; Coudray, N.; Jour, G.; Dawood, Z.; Hong, R.; Esteva, E.; Sakellaropoulos, T.; Donnelly, D.; Moran, U.; et al. Deep Learning and Pathomics Analyses Reveal Cell Nuclei as Important Features for Mutation Prediction of BRAF-Mutated Melanomas. *J. Investig. Dermatol.* **2022**, *142*, 1650–1658.e6. [CrossRef] [PubMed]
43. Saldanha, O.L.; Quirke, P.; West, N.P.; James, J.A.; Loughrey, M.B.; Grabsch, H.I.; Salto-Tellez, M.; Alwers, E.; Cifci, D.; Ghaffari Laleh, N.; et al. Swarm learning for decentralized artificial intelligence in cancer histopathology. *Nat. Med.* **2022**, *28*, 1232–1239. [CrossRef] [PubMed]
44. Haghighat, M.; Browning, L.; Sirinukunwattana, K.; Malacrino, S.; Khalid Alham, N.; Colling, R.; Cui, Y.; Rakha, E.; Hamdy, F.C.; Verrill, C.; et al. Automated quality assessment of large digitised histology cohorts by artificial intelligence. *Sci. Rep.* **2022**, *12*, 5002. [CrossRef]
45. Salvi, M.; Acharya, U.R.; Molinari, F.; Meiburger, K.M. The impact of pre- and post-image processing techniques on deep learning frameworks: A comprehensive review for digital pathology image analysis. *Comput. Biol. Med.* **2021**, *128*, 104129. [CrossRef] [PubMed]
46. Campanella, G.; Hanna, M.G.; Geneslaw, L.; Miraflor, A.; Werneck Krauss Silva, V.; Busam, K.J.; Brogi, E.; Reuter, V.E.; Klimstra, D.S.; Fuchs, T.J. Clinical-grade computational pathology using weakly supervised deep learning on whole slide images. *Nat. Med.* **2019**, *25*, 1301–1309. [CrossRef]
47. Terada, Y.; Takahashi, T.; Hayakawa, T.; Ono, A.; Kawata, T.; Isaka, M.; Muramatsu, K.; Tone, K.; Kodama, H.; Imai, T.; et al. Artificial Intelligence-Powered Prediction of ALK Gene Rearrangement in Patients with Non–Small-Cell Lung Cancer. *JCO Clin. Cancer Inform.* **2022**, *6*, e2200070. [CrossRef]
48. Nero, C.; Boldrini, L.; Lenkowicz, J.; Giudice, M.T.; Piermattei, A.; Inzani, F.; Pasciuto, T.; Minucci, A.; Fagotti, A.; Zannoni, G.; et al. Deep-Learning to Predict BRCA Mutation and Survival from Digital H&E Slides of Epithelial Ovarian Cancer. *Int. J. Mol. Sci.* **2022**, *23*, 11326. [CrossRef]
49. Yamashita, R.; Long, J.; Longacre, T.; Peng, L.; Berry, G.; Martin, B.; Higgins, J.; Rubin, D.L.; Shen, J. Deep learning model for the prediction of microsatellite instability in colorectal cancer: A diagnostic study. *Lancet Oncol.* **2021**, *22*, 132–141. [CrossRef]
50. Linder, N.; Konsti, J.; Turkki, R.; Rahtu, E.; Lundin, M.; Nordling, S.; Haglund, C.; Ahonen, T.; Pietikäinen, M.; Lundin, J. Identification of tumor epithelium and stroma in tissue microarrays using texture analysis. *Diagn. Pathol.* **2012**, *7*, 22. [CrossRef]
51. Bradish, J.R.; Richey, J.D.; Post, K.M.; Meehan, K.; Sen, J.D.; Malek, A.J.; Katona, T.M.; Warren, S.; Logan, T.F.; Fecher, L.A.; et al. Discordancy in BRAF mutations among primary and metastatic melanoma lesions: Clinical implications for targeted therapy. *Mod. Pathol.* **2015**, *28*, 480–486. [CrossRef]
52. Long, G.V.; Stroyakovskiy, D.; Gogas, H.; Levchenko, E.; de Braud, F.; Larkin, J.; Garbe, C.; Jouary, T.; Hauschild, A.; Grob, J.J.; et al. Combined BRAF and MEK Inhibition versus BRAF Inhibition Alone in Melanoma. *N. Engl. J. Med.* **2014**, *371*, 1877–1888. [CrossRef] [PubMed]
53. Rossman, P.; Zabka, T.S.; Ruple, A.; Tuerck, D.; Ramos-Vara, J.A.; Liu, L.; Mohallem, R.; Merchant, M.; Franco, J.; Fulkerson, C.M.; et al. Phase I/II trial of vemurafenib in dogs with naturally occurring, BRAF-mutated urothelial carcinoma. *Mol. Cancer Ther.* **2021**, *20*, 2177–2188. [CrossRef] [PubMed]
54. Tagawa, M.; Tambo, N.; Maezawa, M.; Tomihari, M.; Watanabe, K.I.; Inokuma, H.; Miyahara, K. Quantitative analysis of the BRAF V595E mutation in plasma cell-free DNA from dogs with urothelial carcinoma. *PLoS ONE* **2020**, *15*, e0232365. [CrossRef] [PubMed]
55. Aupperle-Lellbach, H.; Grassinger, J.; Hohloch, C.; Kehl, A.; Pantke, P. Diagnostische Aussagekraft der BRAF-Mutation V595E in Urinproben, Ausstrichen und Bioptaten beim kaninen Übergangszellkarzinom. *Tierärztliche Prax. Ausg. K Kleintiere Heimtiere* **2018**, *46*, 289–295. [CrossRef]
56. Wu, S.; Hong, G.; Xu, A.; Zeng, H.; Chen, X.; Wang, Y.; Luo, Y.; Wu, P.; Liu, C.; Jiang, N.; et al. Artificial intelligence-based model for lymph node metastases detection on whole slide images in bladder cancer: A retrospective, multicentre, diagnostic study. *Lancet Oncol.* **2023**, *24*, 360–370. [CrossRef]
57. Fell, C.; Mohammadi, M.; Morrison, D.; Arandjelovic´, O.; Syed, S.; Konanahalli, P.; Bell, S.; Bryson, G.; Harrison, D.J.; Harris-Birtill, D. Detection of malignancy in whole slide images of endometrial cancer biopsies using artificial intelligence. *PLoS ONE* **2023**, *18*, e0282577. [CrossRef]
58. Bhinder, B.; Gilvary, C.; Madhukar, N.S.; Elemento, O. Artifi Cial intelligence in cancer research and precision medicine. *Cancer Discov.* **2021**, *11*, 900–915. [CrossRef]
59. Borhani, S.; Borhani, R.; Kajdacsy-Balla, A. Artificial intelligence: A promising frontier in bladder cancer diagnosis and outcome prediction. *Crit. Rev. Oncol. Hematol.* **2022**, *171*, 103601. [CrossRef] [PubMed]

60. Lebret, T.; Pignot, G.; Colombel, M.; Guy, L.; Rebillard, X.; Savareux, L.; Roumigue, M.; Nivet, S.; Coutade Saidi, M.; Piaton, E.; et al. Artificial intelligence to improve cytology performances in bladder carcinoma detection: Results of the VisioCyt test. *BJU Int.* **2022**, *129*, 356–363. [CrossRef]

Received: 20 January 2024 | Revised: 11 April 2024 | Accepted: 12 April 2024

DOI: 10.1111/vco.12978

ORIGINAL ARTICLE

Veterinary and Comparative Oncology WILEY

Effective detection of *BRAF*^{V595E} mutation in canine urothelial and prostate carcinomas using immunohistochemistry

Leonore Aeschlimann[1] | Alexandra Kehl[2,3] | Franco Guscetti[4] | Caroline Posthaus[1] | Heike Aupperle-Lellbach[2,3] | Sven Rottenberg[1] | Simone de Brot[1,5]

[1]Institute of Animal Pathology, University of Bern, Bern, Switzerland

[2]Laboklin GmbH & Co. KG, Bad Kissingen, Germany

[3]Technical University of Munich, School of Medicine, Institute of Pathology, Munich, Germany

[4]Institute of Veterinary Pathology, University of Zurich, Zurich, Switzerland

[5]School of Veterinary Medicine and Science, University of Nottingham, Sutton Bonington, UK

Correspondence
Simone de Brot, Institute of Animal Pathology, University of Bern, 3012 Bern, Switzerland.
Email: simone.debrot@unibe.ch

Funding information
Albert Heim Foundation, Grant/Award Number: 148

Abstract

Canine urothelial carcinoma (UC) and prostate carcinoma (PC) frequently exhibit the *BRAF*^{V595E} mutation, akin to the *BRAF*^{V600E} mutation common in various human cancers. Since the initial discovery of the *BRAF* mutation in canine cancers in 2015, PCR has been the standard method for its detection in both liquid and tissue biopsies. Considering the similarity between the canine *BRAF*^{V595E} and human *BRAF*^{V600E} mutations, we hypothesized that immunohistochemistry (IHC) using a BRAF^{V600E}-specific antibody could effectively identify the canine mutant BRAF^{V595E} protein. We tested 122 canine UC (bladder $n = 108$, urethra $n = 14$), 21 PC, and benign tissue using IHC and performed digital droplet PCR (ddPCR) on all 122 UC and on 14 IHC positive PC cases. The results from ddPCR and IHC were concordant in 99% (135/136) of the tumours. Using IHC, *BRAF*^{V595E} was detected in 72/122 (59%) UC and 14/21 (65%) PC. Staining of all benign bladder and prostate tissues was negative. If present, mutant BRAF staining was homoge- nous, with rare intratumour heterogeneity in three (4%) cases of UC. Additionally, the *BRAF*^{V595E} mutation was more prevalent in tumours with urothelial morphol- ogy, and less common in glandular PC or UC with divergent differentiation. This study establishes that BRAF^{V600}-specific IHC is a reliable and accurate method for detecting the mutant *BRAF*^{V595E} protein in canine UC and PC. Moreover, the use of IHC, especially with tissue microarrays, provides a cost-efficient test for large-scale screening of canine cancers for the presence of *BRAF* mutations. This advancement paves the way for further research to define the prognostic and predictive role of this tumour marker in dogs and use IHC to stratify dogs for the treatment with BRAF inhibitors.

KEYWORDS
BRAF, canine, immunohistochemistry, prostate carcinoma, urothelial carcinoma

1 | INTRODUCTION

Urothelial carcinoma (UC) of the bladder and urethra is the most common lower urinary tract tumour in dogs.[1-3] Due to the propensity of distant metastases and the anatomic location, the long term prognosis is poor and cure is rare; however, many dogs with UC that receive treatment can have improved quality for relatively long periods of time.[1,2]

There is a significant predisposition for Scottish Terriers, West Highland White Terriers, Shelties and others breeds for tumour development, and other risk factors include female sex and being spayed or neutered.[3-6] The high breed predisposition indicates an underlying genetic basis for the disease.[3,6-9] In multiple studies, the activating *BRAF*^{V595E} mutation, the canine homologue of human *BRAF*^{V600E}, was identified as somatic driver mutation to be frequently present in 65%–87% of UC of dogs.[1,5,6,8,10,11] BRAF is a serine-threonine pro- tein kinase and immediate downstream effector of RAS. It activates the MAP kinase extracellular signal regulated kinase (MEK), which then phosphorylates extracellular signal-regulated kinases 1 and 2 (ERK1 and ERK2), and thereby orchestrates cell growth, differentia- tion, proliferation, senescence and apoptosis.[12]

In humans, the activating *BRAF*^{V600E} mutation is particularly prev- alent in melanoma, where it is present in nearly half of the cases.[13] It significantly increases protein kinase activity, resulting in constitutive BRAF-MEK-ERK signalling that drives tumour growth.[14] The high frequency of the *BRAF*^{V600E} mutations in melanoma and other human cancers, including colorectal and thyroid carcinoma, implies that this oncogene may be an attractive therapeutic target. Indeed, in recent years, various inhibitors that specifically target *BRAF*^{V600E} mutations (e.g., vemurafenib, dabrafenib and encorafenib) have successfully entered the clinic.[14] Hence, in addition to being a diagnostic and prognostic marker, the *BRAF* mutation has also predictive relevance.[15,16]

Interestingly, canine UC and human muscle-invasive bladder can- cer share many similarities at the cellular and molecular level, with similar propensity and site of metastases, as well as response to therapy.[1,3,4,17,18] The dog is therefore considered a highly relevant animal model for studies of human UC.[3,11] However, in contrast to dogs, *BRAF* mutations are only sporadically described in human muscle-invasive UC.[11,17,19]

In canine cancers, the *BRAF*^{V595E} mutation is not only prevalent in UC of the bladder and urethra but also in prostatic carcinomas (PC),[6,20] while it remains absent in other investigated canine cancer types.[6] Canine PC shares the high metastatic potential and invasive nature with UC.[21] It may also originate from various epithelial tissues in the prostate, mirroring human prostate cancer.[22] The exact cellular origin of canine prostate cancer often remains elusive due to small biopsy samples and the complex nature of these tumours character- ized by varied differentiation, significant inflammation and necrosis.[23] This complexity raises questions about the exact role of the *BRAF*^{V595E} mutation in canine prostate tumours: is it a characteristic of UC in the prostatic urethra, true prostate adenocarcinoma or both?[8,20]

For the detection of *BRAF* mutations in human cancer multiple methods exist, including Sanger sequencing, pyrosequencing, next-generation sequencing, immunohistochemistry (IHC) and PCR.[24-26] Test sensitivity, specificity, cost, turnaround time and requirements for equipment and experienced staff vary between the different methods. Most commonly, initial detection of cases with *BRAF*^{V600E} or its corresponding mutant protein is performed by IHC, in combination with a molecular test.

In contrast, in dogs, PCR, either quantitative (qPCR) or digital (dPCR), is currently the only well-established method to detect the *BRAF*^{V595E} mutation.[20,27] Both PCR techniques are highly specific, however, dPCR outperforms qPCR due to its higher sensitivity.[28] PCR can be performed using liquid or tissue biopsies, including urine, cytologic smears or formalin-fixed paraffin-embedded (FFPE) material.[29] However, as with any diagnostic tool, there are certain limitations. The specific PCR for detecting *BRAF*^{V595E} is not available in all diagnostic institutions and alternative test methods for canine samples are currently lacking. For screening a larger series of cases by PCR, sample pooling is possible, but does not allow to separate test results for the individual cases. Furthermore, spatial analysis of the mutation, including the evaluation of intratumour heterogeneity or the correlation of mutation with defined histopathologic features, is not possible using PCR. IHC provides a cost-efficient and widely established alternative test method to address these limitations. Indeed, IHC is one of the most frequently used methods for the evaluation of *BRAF*^{V600E} mutation status in human medicine, and is especially valuable because it provides spatial information and can detect intratumoural heterogeneity.[30]

Studies reporting the performance of IHC for mutated BRAF pro- tein detection are currently lacking in the veterinary literature. Due to the homologous mutation of canine and human BRAF, we hypothe- sized that IHC for anti-human BRAF^{V600E} protein would reliably detect BRAF^{V595E} protein in canine tissue. In order to investigate this, we evaluated 143 cases of canine UC and PC with different mutation status by IHC and compared these results with the corresponding dig- ital droplet PCR (ddPCR) test results.

2 | MATERIALS AND METHODS

2.1 | Samples

FFPE canine tissue of 108 bladder UC, 14 urethra UC, 21 PC (pros- tatic urethral UC and prostatic adenocarcinomas) and 60 benign pros- tate were included (normal mature $n = 11$; normal pre-puberty $n = 15$; prostatitis $n = 11$; hyperplasia $n = 11$; castration induced atrophy $n = 12$). In 30 and one cases of UC and PC, respectively, benign tissue was also available adjacent to tumour tissue, which included benign urothelium or non-neoplastic prostate gland. For all cases, FFPE tissue blocks and tissue microarrays (TMAs) were available. TMAs were created with the TMA Grand Master (3DHistech, Budapest, Hungary) with multiple (1–10) cores for each tumour and core diameters of 0.6 mm. The following case information was provided: age at the time of biopsy sampling, sex, neutering status and dog breed. For UC, the most common breeds were crossbreed

($n = 25$), Labrador Retriever ($n = 12$), Cocker Spaniel ($n = 8$), West Highland White Terrier ($n = 7$), Jack Russell Terrier ($n = 6$), Cavalier King Charles Spaniel ($n = 6$), and Scottish Terrier ($n = 5$) (complete breed list provided as supporting information). Out of 122 UC cases, 83 (68%) dogs were female (63 neutered, 2 intact, 18 of unknown neutering status), 39 (32%) were male (22 neutered, 3 intact, 14 of unknown neutering status). The mean age at diagnosis was 10 years (range 4–14 years). For prostate tumours, the following breeds were represented: Labrador Retriever ($n = 8$), Jack Russell Terrier ($n = 2$), Yorkshire Terrier ($n = 2$), Cross breed ($n = 2$), Fox Terrier ($n = 1$), Staffordshire Bullterrier ($n = 1$), Welsh Corgi ($n = 1$), Rottweiler ($n = 1$), Border Collie ($n = 1$) and Belgian Shepherd ($n = 1$). Out of 21 PC cases, 16 (80%) dogs were neutered, 3 dogs were intact and one of unknown neutering status. The mean age at diagnosis was 9.5 years (range 6–13 years).

2.2 | Histology

Haematoxylin and eosin (HE) stained tissue sections were prepared from all TMAs and from all corresponding FFPE blocks. Slides were then scanned using the NanoZoomer S360MD Slide scanner system (Hamamatsu Photonics, Shizuoka, Japan) for digital evaluation using the NDP.view2 viewer (HAMAMATSU Photonics K.K., Hamamatsu City, Japan). Bladder and urethral tumours were classified as either low- or high-grade UC based on the most recent canine grading sys- tem of Meuten.[31] Furthermore, these tumours were categorised based on their histomorphology as: (1) conventional urothelial, (2) urothelial with divergent (glandular, squamous or both) differentiation or (3) other (anaplastic or other differentiation). Prostate tumours were categorised based on the most recent classification system by Palmieri et al.[32] as (1) glandular (adenocarcinoma), (2) urothelial or (3) mixed (any combination of urothelial, glandular or other).

2.3 | Immunohistochemistry

IHC was initially performed on TMAs and, in a second step, on 38 ($n = 36$ UC, $n = 2$ PC) corresponding FFPE blocks which showed positive staining on the TMA and which consisted of a large, typically transmural, tumour tissue sample. Tissue blocks were cut using a microtome and mounted on a microscope slide. Briefly, the FFPE tissue was pretreated with ULTRA cell conditioning solution 1 (Tris EDTA) for 72 min at 99°C and was then incubated with the mouse-anti-human primary BRAF V600E mutation specific (VE1) antibody from Roche Diagnostics (material number: 08033706001, catalogue number: 760-5095) for 60 min at 36°C. For detection, the OptiView DAB IHC Detection Kit (Ventana Medical Systems, Roche, Basel, Switzerland) was used according to the manufacturer's instructions. Slides were then scanned, and digitally reviewed (same scanner and software as indicated above). The immunostaining was localized to the cytoplasm and was categorised as either absent or present. Intra- tumour staining was classified as either homogeneous (distributed regularly and evenly throughout the tumour tissue) or heterogeneous (regional staining differences with focal or multifocal negative areas). Non-neoplastic tissues as indicated above served as (internal) negative control. Tissue from *BRAF*^{V600E} mutated human colon carcinoma was used as a positive control. For the validation of IHC positive canine cases, ddPCR was performed individually for each case.

2.4 | Digital droplet PCR

In a first step, ddPCR was performed on all UC of the bladder and urethra, independent of their IHC staining result. Based on the high concordance of IHC and ddPCR in the UC cases, only IHC positive prostate tumours were tested with ddPCR. For DNA extraction,

3 x 10 µm sections were prepared from the FFPE full tissue blocks. The extraction was performed using the QIAamp® DNA FFPE Tissue Kit (Qiagen, Hilden, Germany) according to the manufacturer's instructions. Isolated DNA was examined for the presence of the BRAF mutation c.1784T > A by ddPCR using a mutation-specific TaqMan® assay as described by Mochizuki et al.[20] Analysis was performed using the DropletReader (Bio-Rad, Feldkirchen, Germany) and the QuantaSoft™ Software (Bio-Rad, Feldkirchen, Germany). For bladder and urethra UC with negative IHC result, ddPCR was performed in pools of two. If the result from the pool was positive, the ddPCR was repeated on the individual tissue blocks.

2.5 | Statistical analysis

Statistical analysis was performed with NCSS 2023 (23.0.2) software. Pearson's Chi-Square test was performed to test for association of *BRAF* mutation with tumour classification, neutering, sex and tissue type; two-sample *t*-test was performed to test for differences in age of dogs with *BRAF*-mutated versus non-mutated tumours. $p < .05$ was considered statistically significant.

3 | RESULTS

3.1 | Histology

All bladder and urethra tumours were defined as high-grade carcinoma, except for one case of low-grade bladder UC in an 8-years-old male intact Labrador Retriever. The majority of these tumours corresponded to a conventional UC (90/122; 74%). Half of the remaining cases presented either as UC with divergent, squamous or glandular, differentiation (16/122; 13%), or as non-urothelial or poorly differentiated tumours (16/122; 13%). Inflammation of the tumour stroma was common (108/122; 89%), characterized by a multifocal predomi- nantly lymphoplasmacytic infiltrate of variable severity, with occa- sional formation of lymphoid follicles. In transmural samples, invasion into the muscular layer was observed in 20/40 (50%) cases. The majority of prostate tumours were categorised as mixed carcinoma

given their heterogeneous glandular, urothelial or poorly differentiated histomorphology (10/21; 48%). Remaining cases were approximately equally either UC (6/21; 29%) or prostatic adenocarcinoma with predominance of neoplastic acini, glands or ducts (5/21; 24%). As for the bladder and urethra tumours, stromal inflammation was fre- quent and consisted of a mixed population neutrophils and mononu- clear leukocytes (18/21; 90%).

3.2 | BRAF V600E IHC

Following the identical antigen retrieval and staining protocol as recommended for human tissue, canine tissue was immunolabelled with a mutation-specific mouse monoclonal antibody that was raised against a synthetic peptide representing the $BRAF^{V600E}$ mutated amino acid sequence from amino acids 596–606. The sequence of this peptide (GLATEKSRWSG) is identical to the canine $BRAF^{V595E}$ protein.[9] The IHC staining allowed direct visualization of the mutant protein in the tumour tissue, at single-cell resolution. In contrast to the wild-type protein which is located intranuclear, mutant BRAF is expressed in the cytoplasm, which was confirmed by the performed IHC staining in all cases. Out of 122 cases of bladder and urethra UC, 70 (57%) were positive for $BRAF^{V600E}$ IHC (Table 1). The majority of conventional UC stained positive (62/90; 69%), whereas the opposite was true for UC with divergent (7/16; 44%) or non-urothelial differentiation (1/16; 6%). Positive immunolabelling was characterized as homogeneous cytoplasmic, variably intense, staining of tumour cells with sharp demarcation to surrounding non-neoplastic tissue, which remained unstained (Figure 1). The transition of malignant to benign tissue was available in 28 out of 70 IHC positive cases and the highly specific staining of tumour cells was confirmed in all cases. Intratumour staining was homogenous in all but three tumours, where immunolabelling was more heterogeneous, with multifocal negative areas or variations in staining intensity. In two of these cases, staining variation corresponded to different histomorphological differentiation, with positive staining for urothelial morphology and negative staining in regions with divergent, non-urothelial differentiation. The third tumour with heterogeneous immunostaining had diffuse urothelial morphology and staining variation could not be

Bladder and urethra carcinoma		ddPCR		
Histological subtype	IHC	Positive	Negative	Total
Conventional urothelial	Positive	62	0	62
	Negative	1	27	28
Urothelial with divergent differentiation	Positive	7	0	7
	Negative	0	9	9
Non-urothelial or poorly differentiated	Positive	1	0	1
	Negative	0	15	15
Total		71	51	122

Abbreviations: ddPCR, digital droplet PCR; IHC, immunohistochemistry.

TABLE 1 $BRAF^{V595E}$ mutation status of canine bladder and urethra tumours tested by ddPCR and IHC. All cases with positive IHC were confirmed by ddPCR with consistent results. One small sample of bladder UC stained negative with IHC, but was found to be BRAF mutated by ddPCR.

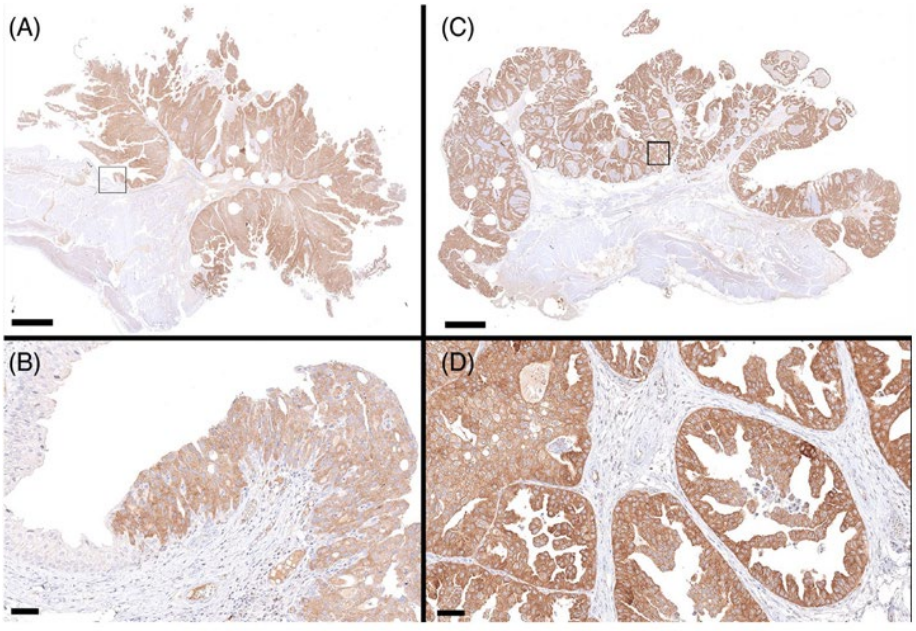

FIGURE 1 Two cases of $BRAF^{V595E}$ mutated canine bladder urothelial carcinoma with diffuse cytoplasmic staining, $BRAF^{V600E}$ immunohistochemistry. (A) Overview of the first case, size bar indicates 2.5 mm. (B) Higher magnification of (A), showing the transition of tumour to benign tissue demonstrating highly specific staining of tumour cells with negative staining of adjacent benign urothelium. Size bar indicates 50 μm. (C) Overview of the second case, size bar indicates 2.5 mm. (D) Higher magnification of (C), size bar indicates 50 μm.

explained by variation in tumour morphology. The single case with low-grade UC had negative IHC staining.

Out of 21 PC, 14 (65%) were positive by IHC, with homogenous intratumour staining of glandular, urothelial and mixed carcinomas (Table 2). All tested benign prostate tissues (n = 60) stained negative (Figure 2). Occasional non-specific IHC staining was seen in low numbers of stromal leukocytes, predominantly plasma cells, characterized by weak cytoplasmic immunolabelling.

TABLE 2 *BRAF*^{V595E} mutation status of benign and malignant canine prostate tissue tested by ddPCR and IHC. All cases with positive IHC were confirmed by ddPCR with consistent results.

		ddPCR			
Prostate lesion	IHC	Positive	Negative	NP	Total
Adenocarcinoma	Positive	1	0		1
	Negative			4	4
Urothelial carcinoma	Positive	5	0		5
	Negative			1	1
Mixed carcinoma	Positive	8	0		8
	Negative			2	2
Non-neoplastic	Positive				0
	Negative			65	65
Total		14	0	72	86

Abbreviations: ddPCR, digital droplet PCR; IHC, immunohistochemistry; NP, not performed.

3.3 | digital droplet PCR

All 122 bladder and urethra UC were tested by ddPCR, which confirmed a high specificity (100%) and sensitivity (99%) of the BRAF IHC (Table 1). All 70 cases with positive IHC staining were confirmed to be BRAF mutated by ddPCR. Out of 52 UC with negative IHC, 51 cases were con- firmed to be negative by ddPCR. The one remaining IHC negative tumour, which was tested BRAF positive by ddPCR consisted of a very small tis- sue sample of a conventional bladder UC. All 14 PC with positive IHC were confirmed to bear the *BRAF*^{V595E} mutation by ddPCR.

3.4 | Correlation BRAF mutation with tumour type, sex, neutering and breed

Bladder and urethra tumours with conventional urothelial differentiation were more likely to be *BRAF*-mutated compared to UC with

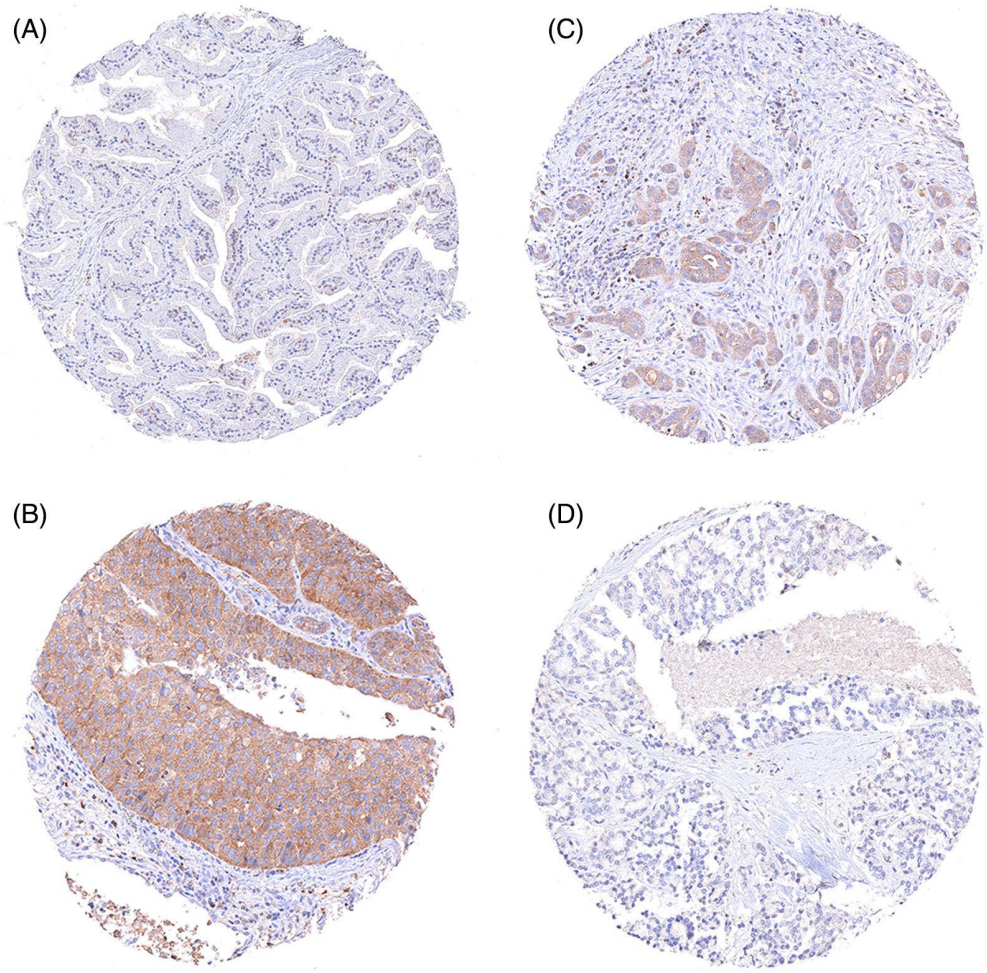

FIGURE 2 Canine tissue microarray cores of benign prostate (A) and prostate carcinoma (PC) (B–D), *BRAF*^{V600E} immunohistochemistry.
(A) Normal prostate with negative staining, (B) BRAF mutated PC with diffuse cytoplasmic staining,
(C) Highly invasive BRAF mutated PC with positive staining, and
(D) BRAF non-mutated PC with negative staining.

divergent or tumours with non-urothelial histomorphology ($p < .0001$). No correlation was found between sex, castration status, tissue type (bladder vs. urethra), age, breed and this specific mutation.

BRAF mutated PC was only observed in castrated dogs ($n = 14$), whereas prostate tumours of entire dogs lacked this specific mutation ($n = 4$). Two of the remaining three cases of non-mutated PC were found in neutered dogs of the same breed (Yorkshire terrier). Despite limitation due to low case numbers, *BRAF* mutation was confirmed to be associated with castration ($p < .01$).

Following the same trend as bladder and urethra tumours, pros- tate carcinomas (PC) with urothelial differentiation (UC or mixed) were more likely to be *BRAF* mutated ($p < .05$).

4 | DISCUSSION

In our study, we established that an anti-human $BRAF^{V600E}$ IHC is a reliable and accurate method for detecting the mutant $BRAF^{V595E}$ protein in canine UC and PC. IHC provides a cost-effective and familiar approach for pathologists, regularly used in human cancer diagnostics to identify the $BRAF^{V600E}$ mutation.[26,33] For dogs, however, mutation-specific BRAF IHC has not yet been set up and canine studies investigating mutant BRAF protein expression in tissue are currently not available in the literature. Given the genetic similarity of the *BRAF* mutations in dogs and humans, we hypothesized that the mutated protein is detected in canine UC and PC using a human anti- $BRAF^{V600E}$ IHC protocol. This hypothesis was confirmed by our paral- lel testing of 143 canine cases with ddPCR, demonstrating a 100% specificity and a high sensitivity (99%) of the $BRAF^{V600E}$ IHC for detecting the $BRAF^{V595E}$ mutant protein in canine urothelial and pros- tate tumours. The one case of UC with a negative IHC and a positive ddPCR test result consisted of a very small tumour sample, which might explain the lack of staining.

In human cancers, the presence of $BRAF^{V600E}$ has been reported to correlate with specific histomorphological tumour subtypes. For instance, in thyroid cancer, it is strongly linked with either the papillary or anaplastic morphology,[34] and in melanomas, it is associated with pigmentation, scatter of intraepidermal melanocytes and solar elastosis.[35] Our recent study using artificial intelligence to analyse canine urinary bladder tumours revealed that *BRAF* mutations in these cases frequently corresponded with papillary growth, smooth and pushing rather than invasive tumour fronts.[7] The present investigations support a parallel between the morphological implications of BRAF mutations in both human and canine cancers. In contrast, Yamasaki and colleagues' recent investigation into the cytomorphological differences in UC cell lines with and without the $BRAF^{V595E}$ mutation found no significant variances.[36] This suggests that in vivo morphologies may be influenced by the tumour microenvironment or obscured in vitro by cell culture conditions.

In the present study, 72/122 (59%) UC and 13/21 (65%) PC were $BRAF^{V595E}$ mutated. This is in accordance with the prevalence of the mutation reported in the literature using PCR,[5-7,9,20] despite our limitation of a small sample size of PC cases. In the dog, $BRAF^{V595E}$ is considered a diagnostic marker for UC and PC.[5,20] However, it is important to keep in mind that the absence of $BRAF^{V59E5}$ does not exclude UC and PC since tumours lacking this specific mutation will not be detected with this method. Therefore, in cases where a tumour of the urinary tract or prostate is suspected, but $BRAF^{V595E}$ is absent, other diagnostic tools, for example, cytology, histology or imaging techniques, need to be performed to assess whether a neoplastic process is present or not.

A number of studies have investigated whether $BRAF^{V595E}$ is also prognostic or predictive for UC.[5,37,38] Thus far, none of these studies was able to demonstrate a correlation between *BRAF* mutation status, overall survival, and disease-free interval. This is in contrast to human papillary thyroid carcinomas, where $BRAF^{V600E}$ has been shown to be significantly associated with increased cancer-related mortality.[15] A large retrospective study on human melanomas also found that the $BRAF^{V600E}$ mutation is associated with increased mortality.[39]

The therapeutic implications of BRAF mutations are noteworthy. BRAF inhibitors (BRAFi), including vemurafenib and dabrafenib, have shown significant clinical benefits in human patients with $BRAF^{V600E}$ mutant cancer and have been approved by the FDA.[40,41] However, the efficacy of BRAFi varies across different cancer types and therapy resistance remains a major challenge. Recently, combination therapies with MEK and/or EGFR inhibitors have gained attention due to their improved performance compared to BRAFi monotherapy. To evaluate the predictive relevance of $BRAF^{V595E}$ in dogs, BRAFi have been tested in canine patients with naturally occurring *BRAF*-mutated UC and a few canine UC cell lines with or without *BRAF* mutation. Ross- man et al. performed a clinical trial with vemurafenib in 34 pet dogs with BRAF mutant UC.[42] Treatment led to partial remission in 9 out of 24 dogs, with a median progression-free interval of 181 days. The responses to this BRAF inhibitor in dogs did mimic those reported in men, including good initial response, followed by drug resistance. Maeda et al. tested the effect of dabrafenib on two different canine UC cell lines with mutant or wild-type BRAF.[38] This drug was shown to be effective in BRAF mutant but not wild-type tumour cells. How- ever, both cell lines were relatively resistant to this BRAF inhibitor. Jung et al. compared the anti-tumour effect of sorafenib and vemura- fenib in three canine and one human BRAF mutated TCC cell lines. In contrast to human tumours and the one investigated human cell line in their study, canine cell lines were more sensitive to sorafenib than vemurafenib.[10] Sorafenib is an important drug for liver cancer therapy in men, primarily through the induction of apoptosis and ferroptosis and it is not a specific BRAF inhibitor, in contrast to vemurafenib.[43] As Jung and colleagues suggest, the different sensitivity of BRAF mutant cancer to sorafenib and vemurafenib in men and dogs may indicate different cancer genetics in men and dogs, innate resistance to vemurafenib in canines, or different drug binding affinity to the BRAF protein in humans and dogs. Variable effects of vemurafenib have already been observed in previous canine UC cell line studies. Decker et al. investigated three BRAF mutants and one wild-type canine UC cell line.[9] Two of three mutant cell lines displayed a clear reduction in pMEK after exposure to vemurafenib, whereas levels of pMEK remained high in the remaining mutant cell line. The wild-type

cell line, which was the same as used by Maeda et al., was characterized by low pMEK levels and no response to vemurafenib. Cronise et al. found BRAF mutant canine UC cell lines to be insensitive to vemurafenib, however MAPK inhibitors were effective in mutant and BRAF wild-type cell lines.[44] Furthermore, ErbB inhibitors were identified to have a synergistic effect with MAPK inhibitors, promoting combination therapies for canine UC.

Noteworthy, efficacy of, and resistance to BRAF/MAPK pathway targeted therapies may potentially be influenced by intratumour *BRAF* mutation heterogeneity. Tumour heterogeneity for mutant BRAF is described to occur in 3% to 15% of melanomas.[45] Whether mutant *BRAF* heterogeneity influences patient outcomes or the response to BRAF/MEK inhibitors in human melanoma remains controversial in the literature.[46,47] While this heterogeneity's impact on patient out- comes in human melanoma is debated, it appears to be a rare occur- rence in canine cancers, based on our findings.

The $BRAF^{V600E}$ mutation has been confirmed to be linked to malignant transformation and is known to be one of the earliest events in tumorigenesis.[48] Of note, this mutation is not purely restricted to malignant lesions, but it is also found in benign tissue changes such as melanocytic nevi, endosalpingiosis and Langerhans cell histiocytosis.[49] It is therefore key, as for any molecular test, that the *BRAF* mutation status is interpreted together with histopathology and clinical information. Thus far, canine $BRAF^{V595E}$ is considered cancer-specific and has not yet been detected in benign tissue.[29,50] This is also consistent with our results from the prostate, where all non-neoplastic prostate samples were negative for $BRAF^{V595E}$ on IHC. However, as mentioned before, a limitation of this study is that non-neoplastic lesions of the lower urinary tract, for example, cystitis was not specifically examined.

The detection of *BRAF* mutations, including the canine-specific $BRAF^{V595E}$, represents one important method for cancer diagnosis, in addition to traditional diagnostic approaches like histology, cytology and imaging. With the establishment of a $BRAF^{V595E}$-specific IHC for canine tissue, we now have a cost-efficient and readily available test for detecting these mutations. While BRAF-targeting therapies in dogs are still evolving, the utility of knowing the BRAF mutation sta- tus in patients with confirmed cancer may be useful to stratify patients for such targeted therapy.

In conclusion, IHC represents a reliable, highly sensitive and spe- cific method to detect mutant $BRAF^{V595E}$ in canine urothelial and prostate tumours. With the availability of TMAs and IHC, cost- efficient testing for large-scale screening of canine cancers for the presence of *BRAF* mutations have become feasible and enable further research to define the prognostic and predictive role of this tumour marker in dogs.

ACKNOWLEDGEMENTS

The authors would like to thank Therese Waldburger and Cristina Graham from the Translational Research Unit of the Univer- sity of Bern for their excellent service in histology, IHC and scanning of the slides. Open access funding provided by Univer- sitat Bern.

FUNDING INFORMATION

Funding for this study was provided by the Albert Heim Foundation (grant number 148).

CONFLICT OF INTEREST STATEMENT

The authors Alexandra Kehl and Heike Aupperle-Lellbach declare no conflict of interest; however, they are employed at LABOKLIN GmbH & Co, which is offering genetic diagnostic tests for routine diagnostics in veterinary medicine. All other authors do not have any conflicts of interest to disclose.

DATA AVAILABILITY STATEMENT

The data that support the findings of this study are available from the corresponding author upon reasonable request.

REFERENCES

1. Knapp DW, Dhawan D, Ramos-Vara JA, et al. Naturally-occurring invasive urothelial carcinoma in dogs, a unique model to drive advances in managing muscle invasive bladder cancer in humans. *Front Oncol*. 2020;9:1493.
2. Fulkerson CM, Knapp DW. Management of transitional cell carcinoma of the urinary bladder in dogs: a review. *Vet J*. 2015;205:217-225.
3. de Brot S, Robinson BD, Scase T, et al. The dog as an animal model for bladder and urethral urothelial carcinoma: comparative epidemiology and histology. *Oncol Lett*. 2018;16:1641-1649.
4. de Brot S, Grau-Roma L, Stirling-Stainsby C, et al. A Fibromyxoid stromal response is associated with muscle invasion in canine urothelial carcinoma. *J Comp Pathol*. 2019;169:35-46.
5. Grassinger JM, Merz S, Aupperle-Lellbach H, Erhard H, Klopfleisch R. Correlation of BRAF variant V595E, breed, histological grade and cyclooxygenase-2 expression in canine transitional cell carcinomas. *Vet Sci*. 2019;6:31.
6. Mochizuki H, Breen M. Comparative aspects of BRAF mutations in canine cancers. *Vet. Sci*. 2015;2:231-245.
7. Küchler L, Posthaus C, Jäger K, et al. Artificial intelligence to predict the BRAF V595E mutation in canine urinary bladder urothelial carcinomas. *Animals*. 2023;13:1-16.
8. Mochizuki H, Kennedy K, Shapiro SG, Breen MB. BRAF mutations in canine cancers. *PLoS One*. 2015;10:1-9.
9. Ostrander E, Decker B, Parker HG, et al. Homologous mutation to human BRAF V600E is common in naturally occurring canine bladder cancer—evidence for a relevant model system and urine-based diagnostic test. *Mol Cancer Res*. 2012;17:1310-1314.
10. Jung H, Bae K, Lee JY, et al. Establishment of canine transitional cell carcinoma cell lines harboring BRAF V595E mutation as a therapeutic target. *Int J Mol Sci*. 2021;22:9151.
11. Wong K, Abascal F, Ludwig L, et al. Cross-species oncogenomics offers insight into human muscle-invasive bladder cancer. *Genome Biol*. 2023;24:1-29.
12. Dhillon AS, Hagan S, Rath O, Kolch W. MAP kinase signalling pathways in cancer. *Oncogene*. 2007;26:3279-3290.
13. Davies H, Bignell GR, Cox C, et al. Mutations of the BRAF gene in human cancer. *Nature*. 2002;417:949-954.
14. Poulikakos PI, Sullivan RJ, Yaeger R. Molecular pathways and mechanisms of BRAF in cancer therapy. *Clin Cancer Res*. 2022;28:4618-4628.
15. Xing M, Alzahrani AS, Carson KA, et al. Association between BRAF V600E mutation and recurrence of papillary thyroid cancer. *J Clin Oncol*. 2015;33:42-50.
16. Araque KA, Gubbi S, Klubo-Gwiezdzinska J. Updates on the management of thyroid cancer. *Horm Metab Res*. 2020;52:562-577.

17. Iyer G, al-Ahmadie H, Schultz N, et al. Prevalence and co-occurrence of actionable genomic alterations in high-grade bladder cancer. *J Clin Oncol*. 2013;31:3133-3140.
18. Boulalas I, Zaravinos A, Delakas D, Spandidos DA. Mutational analysis of the BRAF gene in transitional cell carcinoma of the bladder. *Int J Biol Markers*. 2009;24:17-21.
19. Longo T, McGinley KF, Freedman JA, et al. Targeted exome sequencing of the cancer genome in patients with very high-risk bladder cancer. *Eur Urol*. 2016;70:714-717.
20. Mochizuki H, Shapiro SG, Breen M. Detection of BRAF mutation in urine DNA as a molecular diagnostic for canine urothelial and prostatic carcinoma. *PLoS One*. 2015;10:1-12.
21. Axiak SM, Oncology D, Bigio A. Canine Prostatic Carcinoma. *Compend Contin Educ Vet*. 2012;34:E1-E5.
22. LeRoy BE, Nadella MVP, Toribio RE, Leav I, Rosol TJ. Canine Prostate Carcinomas Express Markers of Urothelial and Prostatic Differentiation. *Vet Pathol*. 2004;140:131-140.
23. de Brot S, Lothion-Roy J, Grau-Roma L, et al. Histological and immunohistochemical investigation of canine prostate carcinoma with identification of common intraductal carcinoma component. *Vet Comp Oncol*. 2022;20:38-49.
24. Mendez LD, Wolsefer NS, Asa SL, Wasman J, Yoest JM, Stojanov IJ. The diagnostic utility of BRAF VE1 mutation-specific immunohistochemistry in ameloblastoma. *Mod Pathol*. 2022;35:1570-1577.
25. Cheng LY, Haydu LE, Song P, et al. High sensitivity sanger sequencing detection of BRAF mutations in metastatic melanoma FFPE tissue specimens. *Sci Rep*. 2021;11:9043.
26. Singarayer R, Mete O, Perrier L, et al. A systematic review and meta-analysis of the diagnostic performance of BRAF V600E immunohistochemistry in thyroid histopathology. *Endocr Pathol*. 2019;30:201-218.
27. Rasteiro AM, Sá E Lemos E, Oliveira PA, Gil da Costa RM. Molecular markers in urinary bladder cancer: applications for diagnosis, prognosis and therapy. *Vet Sci*. 2022;9:107.
28. Gentilini F, Palgrave CJ, Neta M, et al. Validation of a Liquid Biopsy Protocol for Canine BRAFV595E Variant Detection in Dog Urine and its Evaluation as a Diagnostic Test Complementary to Cytology. *Front Vet Sci*. 2022;9:1-11.
29. Aupperle-Lellbach H, Grassinger J, Hohloch C, Kehl A, Pantke P. Diagnostische Aussagekraft der BRAF-Mutation V595E in Urinproben, Ausstrichen und Bioptaten beim kaninen Übergangszellkarzinom. *Tierärztliche Prax Ausgabe K Kleintiere/Heimtiere*. 2018;46:289-295.
30. Ito T, Tanaka Y, Murata M, Kaku-Ito Y, Furue K, Furue M. BRAF Heterogeneity in Melanoma. *Curr Treat Options Oncol*. 2021;22:20.
31. Meuten DJ, Meuten TLK. *Tumors of the Urinary System in Tumors in Domestic Animals*. 5th ed. John Wiley & Sons Inc; 2017.
32. Palmieri C, Foster RA, Grieco V, et al. ScienceDirect histopathological terminology standards for the reporting of prostatic epithelial lesions in dogs. *J Comp Pathol*. 2019;171:30-37.
33. Schirosi L, Strippoli S, Gaudio F, et al. Is immunohistochemistry of BRAF V600E useful as a screening tool and during progression disease of melanoma patients ? *BMC Cancer*. 2016;16:905.
34. Dolezal JM, Trzcinska A, Liao CY, et al. Deep learning prediction of BRAF-RAS gene expression signature identifies noninvasive follicular thyroid neoplasms with papillary-like nuclear features. *Mod Pathol*. 2021;34:862-874.
35. Broekaert SMC, Roy R, Okamoto I, et al. Genetic and morphologic features for melanoma classification. *Pigment Cell Melanoma Res*. 2010;23:763-770.
36. Yamasaki H, Uematsu Y, Okano K, et al. Establishment and characterization of urothelial carcinoma cell lines with and without BRAF mutation (V595E) in dogs. *In Vitro Cell Dev Biol Anim*. 2022;15:898-911.
37. Sakai K, Maeda S, Saeki K, et al. ErbB2 Copy Number Aberration in Canine Urothelial Carcinoma Detected by a Digital Polymerase Chain Reaction Assay. *Vet Pathol*. 2020;57:56-65.
38. Maeda S, Yoshitake R, Chambers JK, et al. BRAF mutation associates CCL17 expression and regulatory T cell recruitment in urothelial car- cinoma of dogs. *Vet Pathol*. 2021;58:971-980.
39. Ny L, Hernberg M, Nyakas M, et al. BRAF mutational status as a prog- nostic marker for survival in malignant melanoma : a systematic review and meta-analysis. *Acta Oncol*. 2020;59:833-844.
40. Atkins MB, Lee SJ, Chmielowski B, et al. Combination Dabrafenib and Trametinib versus combination Nivolumab and Ipilimumab for patients with advanced BRAF -mutant melanoma: the DREAMseq trial - ECOG-ACRIN EA6134. *J Clin Oncol*. 2023;41:186-197.
41. Bouffet E, Hansford JR, Garrè ML, et al. Dabrafenib plus Trametinib in pediatric glioma with BRAF V600 mutations. *N Engl J Med*. 2023; 389:1108-1120.
42. Rossman P, Zabka TS, Ruple A, et al. Phase I/II trial of vemurafenib in dogs with naturally occurring, BRAF-mutated urothelial carcinoma. *Mol Cancer Ther*. 2021;20:2177-2188.
43. Li Q, Chen K, Zhang T, et al. Understanding sorafenib-induced ferrop- tosis and resistance mechanisms: implications for cancer therapy. *Eur J Pharmacol*. 2023;955:175913.
44. Cronise KE, Hernandez BG, Gustafson DL, Duval DL. Identifying the ErbB / MAPK signaling Cascade as a therapeutic target in canine bladder cancer. *Mol Pharmacol*. 2019;96:36-46.
45. Yancovitz M, Litterman A, Yoon J, et al. Intra- and inter-tumor heterogeneity of BRAF V600Emutations in primary and metastatic melanoma. *PLoS One*. 2012;7:1-8.
46. Wilmott JS, Menzies AM, Haydu LE, et al. BRAF V600E protein expression and outcome from BRAF inhibitor treatment in BRAF V600E metastatic melanoma. *Br J Cancer*. 2013;108:924-931.
47. Manfredi L, Meyer N, Tournier E, et al. Highly concordant results between immunohistochemistry and molecular testing of mutated V600E BRAF in primary and metastatic melanoma. *Acta Derm Vener- eol*. 2016;96:630-634.
48. Nikiforova MN, Kimura ET, Gandhi M, et al. BRAF mutations in thyroid tumors are restricted to papillary carcinomas and anaplastic or poorly differentiated carcinomas arising from papillary carcinomas. *J Clin Endocrinol Metab*. 2003;88:5399-5404.
49. Sholl LM. A narrative review of BRAF alterations in human tumors: diagnostic and predictive implications. *Precis Cancer Med*. 2020;3:26.
50. Grassinger J, Gmbh L, Kg C. Nachweis der BRAF-mutation bei kani- nen Prostataerkrankungen detection of BRAF mutation in canine prostatic diseases Einleitung. *Tierarztl Prax Ausg K Kleintiere Heimtiere*. 2019;47:313-320.

SUPPORTING INFORMATION

Additional supporting information can be found online in the Support- ing Information section at the end of this article

Acknowledgements

My special thanks go to Simone: I could not have wished for a better doctoral supervisor, and I am deeply impressed by your knowledge, ambition, kindness and patience. Working with you was a great pleasure and I would do it again and again. I would also like to show my deep appreciation to Sven for all the support, cooperation, and open ears on all matters I could come to you with. I thank the entire Institute of Veterinary Pathology Bern for the collaboration, the pleasant hours during and after work and the friendships that have developed over the years, as well as all co-authors for their valuable contribution to our studies.

My deepest gratitude goes to my husband Marc and our son Louis, who mean the world to me, to my parents-in-law and my father for all the support and good times, and to my sister and my dear friends for all the joy and wonderful moments.

This work is dedicated to Opa Schorsch and Louis.